A COMPUTATIONAL STUDY OF THE COANDA

EFFECT AND ITS IMPLEMENTATION IN

WEB SUPPORT AND TRACTION

By

SATHIA PRABHU THIRUMAL

Bachelor of Engineering
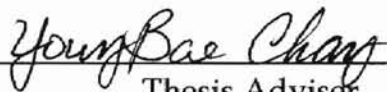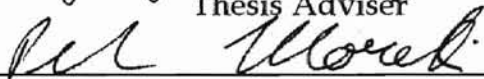
Bharathiar University

Coimbatore, India

1996

Submitted to the Faculty of the
Graduate College of the
Oklahoma State University
in partial fulfillment of
the requirements for
the degree of
MASTER OF SCIENCE
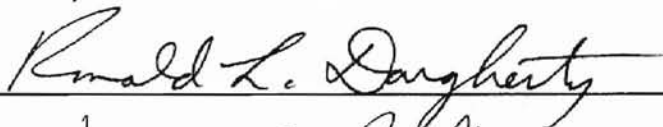May 1998

A COMPUTATIONAL STUDY OF THE COANDA

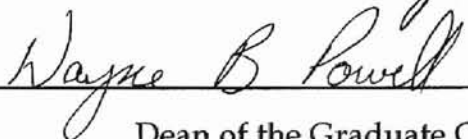# EFFECT AND ITS IMPLEMENTATION IN

WEB SUPPORT AND TRACTION

Thesis Approved:

YoungBae Chang
Thesis Adviser

R. Morel

Ronald L. Daugherty

Wayne B. Powell
Dean of the Graduate College

ii

ACKNOWLEDGMENTS

I wish to express my sincere appreciation and gratitude to my beloved advisor, Dr. Young Bae Chang for his excellent guidance, patience, understanding, and enthusiasm during the entire course of this research work. I am indebted to Dr. Peter M. Moretti for his continuous support and expert guidance throughout the course of this research. I would also like to thank Dr. Ronald L. Dougherty for his suggestions and help.

I wish to take this opportunity to express my gratitude to my beloved parents Mr. T. Sathiamoorthy and Mrs. Usharani Sathiamoorthy, and my brother (Dr.) S. Pradeep for the confidence and moral support they provided during my stay with them and also when I was away from them.

Moreover, I wish to express my appreciation to my friends, Kannan, Rajkumar, Hari, Murali, Vijay Raghavan and Satheesh for giving me great company which made my life at Oklahoma State University a memorable one.

A special thanks goes to Ms. Priya for providing me with all the encouragement and enthusiasm I needed to successfully complete this report.

I wish to express my sincere thanks to the Web handling Research Center at Oklahoma State University for providing continuous financial support during the entire course of this research.

TABLE OF CONTENTS

LIST OF TABLES

LIST OF FIGURES

NOMENCLATURE

b	Nozzle width
R	Radius of curvature of the 90° convex surface
h	Nozzle offset (vertical distance between the start of the curved surface block and the nozzle)
h1	Floatation height (distance between the top of the curved surface block and the web)
ρ	Surface roughness
P	Gauge supply pressure at the inlet of the nozzle
P_1	Upper critical pressure for full attachment
P_2	Lower critical pressure for full separation
μ_t	Turbulent eddy viscosity
ℓ_m	Prandtl's mixing length
k	Turbulent kinetic energy
ε	Turbulent energy dissipation rate

CHAPTER 1
INTRODUCTION

1.1 Background

Thin and flexible materials are called webs, and the methods adopted to handle them are appropriately termed web handling. Web handling can be broadly classified into two types, contact and non-contact methods. Contact methods require firm contact between the rollers and the web during support and transport of webs. At high speeds of operation, the amount of air entrained between the roller and the web can be excessive resulting in slippage between the web and roller surface and damage to the web surface. Also when the web is thin, there is a limit to the tension that can be applied to the web. This also leads to a larger air film thickness, slippage and damage to the web. Contact methods have limitations in handling a coated or printed web, since they may not allow mechanical contact especially when they are wet. These needs have evolved into new techniques of non-contact web handling. Non contact methods of web handling use air jets extensively to support, transport and dry the web.

In general, to increase the productivity, either the line speed or the line width could be increased. However, increasing the line width is prohibitively expensive compared to the boost in productivity. The best way thus is to increase the line speed. However, there are some practical limitations to increasing the line speed. If the line speed is increased, the time the web stays inside the air floatation ovens (used for drying the web) is reduced. This has to be

compensated either by increasing the temperature of the drying air in the oven, by increasing the drying air flow velocity or by increasing the length of the oven.

Sometimes, web flutter occurs in air floatation devices, resulting in damage to the coating on the web. Touchdown is another persistent problem in air-floatation ovens.

1.2 Problem Statement

One of the key phenomena involved in many air floatation devices is the Coanda effect. In order to improve the design of these devices, the behavior of the Coanda air jets should be thoroughly understood.

An extensive literature review reveals that even though abundant work has been done on air jets, they are not directly applicable to web handling. The Coanda effect has been studied by a lot of researchers mostly in relevance to the aerospace industry. Hence it becomes necessary to study the Coanda effect in the context of web handling to reveal the physics behind the current problems in non-contact devices and also to develop new non-contact web handling technologies.

1.3 Objective and Scope of Study

The following points summarize the objectives of this study.

1. To computationally analyze the Coanda air jet in free space to understand the physics involved in the Coanda effect.

2. To computationally analyze the interaction between the Coanda air jet and a stationary rigid web.

3. To develop design and operating guidelines of non-contact devices where the Coanda effect is important.

This study is limited to subsonic air jets, which exit out of a convergent nozzle to follow a 90° convex surface. The atmospheric conditions are considered constant and heat transfer effects are not included in the study model. The air jet-web interaction is studied assuming that the web is stationary, rigid, and perfectly smooth.

CHAPTER 2
LITERATURE REVIEW

Solving a physical problem using analytical and computational methods demands an accurate mathematical description or model, that comprises almost all the factors that influence the problem. An extensive literature review reveals that various statistical methods have been used in similar situations involving turbulent flows. The review has been mostly targeted towards turbulence modeling and its relation to solving jet flows. A brief introduction to turbulence is given as a first step in moving towards the necessity of turbulence modeling.

2.1 Turbulence

While most of us have an intuitive feeling for what turbulence is, it sometimes is difficult to describe turbulence. This results in turbulence often being described by terms like "chaotic" or "random". Nevertheless, we may state some definitive characteristics of turbulence. Turbulence inherently is a three dimensional phenomenon and is largely isotropic, by which we mean that no matter which direction we look at it from, it looks the same. It is made of eddies of widely varying sizes. Another important property of turbulent flows is that it is self-sustaining. The turbulent flow can generate enough "turbulence" to maintain itself producing new eddies to replace those lost due to viscous dissipation. Also, mixing is a very strong phenomenon exhibited by turbulent

flows. Ambient non-turbulent fluid will be strongly entrained into the turbulent flow, increasing the mass flow rate.

One another interesting feature noted by Brown and Roshko (1974) is the presence of coherent structures, as a result of interaction between turbulent and non-turbulent unequal parallel flow. It shows a coherent vortical structure embedded inside random turbulent eddies.

2.2 Need for Turbulence modeling

The need for turbulence modeling arises due to the existence of a wide range of scales of motion. Stated in another way, there is a large variation in the size of the turbulent eddies. A simulation must be able to resolve the smallest sized eddies. For example, if we need to model the turbulent boundary layer, we need to model at least twice the width of the boundary layer, which represents the size of the largest eddy. Within this region we need to model the smallest motion, which can be 1,000 to 1,000,000 times smaller in every direction. This leads to a very large computational domain to solve even for the simplest problems, which is obviously not a practical solution.

Fortunately, almost always we are more interested in the time-averaged effects of turbulence, even if the mean flow is unsteady. And since these time-averaged properties vary more gradually in space, an excessively fine grid is not a requirement. This approach introduces statistical correlations involving fluctuating velocities and temperatures to appear in the conservation equations.

We have no direct way of knowing the magnitude of these terms. We thus have to approximate or "model" these effects in terms of the quantities we can determine. According to Launder and Spalding (1972), a "turbulence model is a set of equations which when solved with the mean flow equations, allows the calculation of the relevant correlations and so simulates the behavior of real fluids in important aspects."

2.3 Development of Turbulence models

Perhaps the first move towards a model of turbulence can be attributed to Boussinesq (1877). He suggested that the effective turbulent shear stress, arising from the cross correlation of fluctuating velocities, could be replaced by the product of the mean velocity gradient and a quantity termed the 'turbulent viscosity' or 'Eddy viscosity', μ_t.

$$-\rho \overline{uv} \equiv \mu_t \frac{\partial U}{\partial y}$$

The turbulent eddy viscosity contains no physical basis, and is purely an arbitrary definition. The reason eddy viscosity concept is useful is that the mean shear and turbulent stresses tend to vary at the same rates so that the variation of the ratio will be slower, and hence easier to model.

The introduction of eddy viscosity provides a framework for constructing a turbulence model, but it does not itself constitute a model. The task of expressing the eddy viscosity in terms of known or calculable quantities still

exists.

Prandtl (1925) was among the first to employ algebraic relations for μ_t, which has been known as the mixing-length hypothesis. He proposed that the eddy viscosity is equal to the local product of the density, magnitude of the mean rate of strain and of the square of a characteristic length scale of the turbulent motion.

$$\mu_t = \rho \ell_m^2 \left| \frac{\partial u}{\partial y} \right|$$

This length scale is called as the mixing length, ℓ_m, and needs to be specified algebraically.

This was followed by an interesting contribution from von Karman (1930). His "similarity hypothesis" removed the need for specifying the mixing-length profile. His analysis implied that the mixing length, ℓ_m, is the ratio of the first to the second spatial derivatives of mean velocity.

$$\mu_t = \rho \ell_m^2 \left| \frac{\partial u}{\partial y} \right|$$

where

$$\ell_m = \frac{\frac{\partial u}{\partial y}}{\frac{\partial^2 u}{\partial y^2}}$$

This model has not been widely accepted because the relationship it predicts for ℓ_m, does not agree with experimental results except in the vicinity of

the wall. Moreover, in turbulent jet flows, at the inflexion points, $\partial^2 u / \partial y^2 = 0$.

This results in an infinite mixing length, hence making this formulation unsuitable to calculate finite shear stresses.

Meanwhile Prandtl (1945) again came up with an improved model, in which he suggested that a more representative velocity scale would be the square root of the turbulent kinetic energy, k. Hence the expression for eddy viscosity became $\mu_t = \rho \sqrt{k} \ell$. The length scale is still prescribed algebraically but the turbulent kinetic energy k, is determined from the solution of a differential equation expressing the processes by which k is transported.

A little earlier, Kolmogorov (1942) had proposed that the character of turbulence could be adequately described by two independent properties. He chose the turbulent kinetic energy k, and the characteristic frequency f, of the energy containing motions. Hence the eddy viscosity term became $\mu_t = \rho \kappa / f$ and the length scale became $\ell = \sqrt{\kappa} / f$. His model was the one of the first two-equation models.

Bradshaw, Ferriss and Atwell (1967) proposed a model which does not have the concept of turbulent eddy viscosity. Their idea was that, if one is prepared to solve the differential equations for turbulence properties, one of these might be for the shear stress itself.

2.4 Wall jets

If we turn our attention to the Coanda air jet technology, there has been a

considerable amount of work done through the years. It all started in 1910 with Henry Coanda's first flight using a jet plane employing the Coanda effect. It was during this flight that the effect was noted by Henry Coanda, as he observed the flames and burned gases remained very close to the fuselage.

Squire (1950) has studied the physics of reattachment of the jet to the surface after a brief separation. He explains that the jet after leaving the nozzle is like a free jet. The highly unstable shear layers on both sides of the jet quickly become turbulent and hence entrain the surrounding fluid closer to the wall. This accelerates the fluid and hence results in a reduced static pressure on the wall. This results in the curving of the jet towards the wall. This only reduces the pressure still more and eventually the jet reattaches to the wall. He also comments on the separation bubble creation during this process.

Bourque and Newman (1960) have compared the theoretical and experimental reattachment of the Coanda air jet to the wall after a brief separation. They have considered a two-dimensional, incompressible jet and an adjacent flat plate. The flat plate is kept close to the jet, at an inclination. They have concluded that the reattachment is primarily due to the entrainment of surrounding air, and the pressure drop it creates in the near-wall region.

The use of Coanda effect for controlling the axisymmetric air jets from the exhaust of VTOL aircraft has been discussed by Felsing and Moller (1969). The interaction between two perpendicular jet streams in the vicinity of a cylindrical

body has been studied. They found that the static pressure of the surface approaches that of the surrounding fluid, immediately after the point of separation. This effect maybe used to control the aircraft.

The bistable behavior of Coanda Jets has been studied by Murai et al. (1989). They found that when the jet flows through a rectangular duct, the attachment or separation prediction depends on the Strouhal number and the shape factor of the duct.

Zhang and Ko (1996) have studied the effect of surface roughness on the jet flow structure and behavior using a smooth and a grooved cylinder. They show that the grooves on the cylinder surface improve reattachment of the air jet.

With the tremendous development in the computing facilities made available for research, the amount of numerical study conducted on air jets has increased manyfold in the recent years. This has brought to light a lot of minute details of flow patterns, thus making refinements to industrial devices like air-turn bars.

CHAPTER 3
COMPUTATIONAL MODELING OF THE
COANDA AIR JET IN FREE SPACE

The computational modeling of the Coanda air jet in free space for the analysis of it's behavior under the influence of various parameters is discussed in detail in this chapter. The parameters studied include the supply pressure, nozzle width, nozzle offset, and the surface roughness of the block. The effects of various computational parameters such as mesh density have also been studied and discussed.

3.1 Computational Model

Solving a physical problem using analytical and computational methods demands an accurate mathematical description or a model, that comprises almost all the factors that influence the problem. The key points that are involved in the development of a computational model to associate the problem in hand are presented below. Fluent/UNS was used as the flow solver.

A detailed discussion of the actual process of creating the model and the grid is presented in the Appendix. Hence we will discuss only about the evolution of the model and how it was used to analyze the behavior of the Coanda jet in free space.

Note that the figures of the model shown below are not to scale. They only attempt to show the various regions that constitute the model.
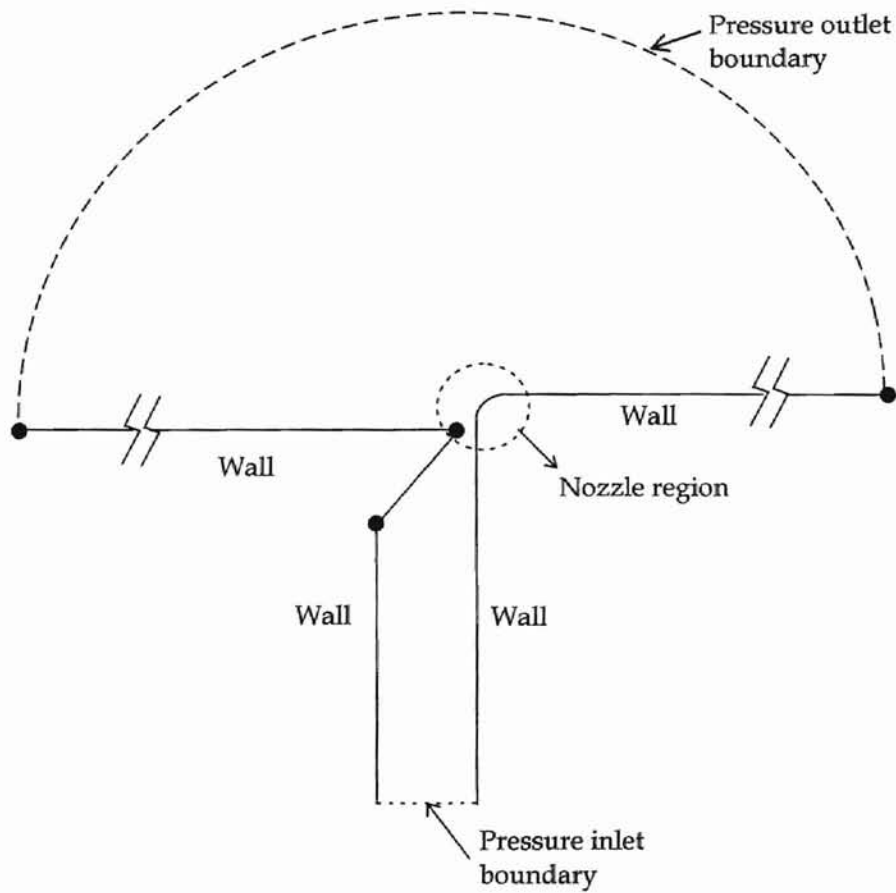
Figure 3.1 Schematic of the computational model for the Coanda air jet in free space
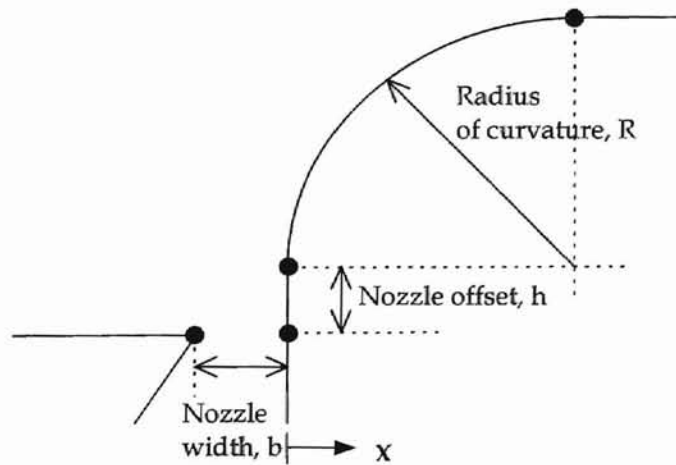
Figure 3.2 Close-up of the nozzle region

One practical difficulty in modeling the free space is the specification of the outlet boundary condition. In the early stage of this study, the model had a relatively small solution domain beyond the nozzle region, i.e., the dome in Fig. 3.1 had a smaller radius. The outlet boundary condition was specified as PRESSURE-OUTLET-BC (maintained at atmospheric pressure to simulate free space) in Fluent/UNS. This boundary was found to constrain and computationally block the jet from exhibiting its behavior freely. This was due to the fact that the pressure at the outlet was being specified equal to the atmospheric pressure, and given the small size of the domain, this boundary conditionwas very unrealistic. So, the dome was increased in size to an extent that it stopped affecting the jet behavior and at the same time provided a closed domain which could model the free space. For all calculations discussed in this chapter, the radius of the half circle which defines the outlet boundary was approximately 90" (2250 mm), while the nozzle width was in the range of 0.01" (0.254 mm) to 0.06" (1.524 mm).

Increasing the size of the computational domain means we have a larger number of grids to solve at. But by using an unstructured triangular grid, the mesh density was suitably varied to maintain a reasonable number of cells in the grid.

3.1.1 Justification of the mesh type

Since the solution domain has a complicated shape especially in the nozzle area, it was decided to use an unstructured mesh, because an unstructured mesh will allow high concentration of the cells in region where high gradients are expected and vice-versa. There are two types of unstructured meshes available in Fluent/UNS : Quadrilateral/Hexahedral element and Triangular/Tetrahedral element.

The triangular elements were chosen for constituting the mesh after considering the factors explained below.

3.1.1.1 Computational expense

When the geometry is complex, the use of triangular elements results in a smaller mesh, compared to when using quadrilateral elements. This is because the triangular mesh allows the cells to be clustered in selected regions whereas in general, the quadrilateral mesh will force the cells to be placed in regions where they are not needed.

Moreover, if the geometry was relatively simple in which the flow would conform to the shape of the geometry, then the quadrilateral elements would have been a better choice because they can accommodate larger cell aspect ratios, which is advantageous in that it can reduce the total number of cells. But, since the geometry under study is sufficiently complex, using

14

quadrilateral elements is not expected to improve the grid quality. Hence it has been decided to use triangular mesh elements.

3.1.1.2 Numerical diffusion

Numerical diffusion is a phenomenon that arises primarily due to truncation errors introduced during computations. It is also sometimes called "false diffusion," because its effect on a flow calculation is analogous to that of increasing the real diffusion coefficient.

One other important factor which influences the numerical diffusion is whether the flow is aligned with the grid or not. When the flow is aligned with the grid, numerical diffusion is reduced. Note that the flow is never aligned if we use triangular meshes. But our need for clustering the cells in the nozzle region while having sparse cells in most other regions outweighs this factor. For complicated swirl flows, even if we use quadrilateral elements, the flow is not aligned with the grid.

One other source of numerical diffusion is the way in which the solution parameters are discretized, especially when the flow is not aligned with the grid. If the parameters are discretized using first-order scheme, then the numerical diffusion is large. This might increase the number of iterations required for convergence. Fluent/UNS recommends the use of second-order discretization for all the solution parameters when using unstructured triangular meshes where, as mentioned earlier, the flow is never aligned with

the grid. Hence, this model employs a second-order discretization scheme for all the solution parameters. Also, the truncation error in the second-order scheme is very low.

3.1.2 Justification of the mesh density

The mesh density is another very important factor that has direct effect on convergence and solution accuracy. With the advent of the unstructured mesh concept, which allows for variable mesh densities at different parts of the domain, lots of care should be taken to decide upon the local mesh density. If the mesh is built coarse, then it will result in the insufficient resolving of the solution gradients, resulting in jumps of the solution between adjacent nodes. This eventually leads to numerical instability and the residuals diverge. On the other hand, if the mesh is made too fine, then it will consume a lot of computer memory and time for the calculation process. Hence, it is essential to strike a balance between the two extreme conditions.

It is a general practice to start with a coarse mesh and refine (or "adapt") the mesh as the solution progresses. Since the study model involves wall jet flows, higher mesh density is required in the near-wall region than in the other fluid regions. In such situations, the Fluent/UNS manual recommends a minimum of 5 cells in any passage to resolve the gradients properly. In our case we have resolved the nozzle region using more than 10 cells.

However, we need to strike a balance at a certain mesh density beyond which any increase in the mesh density does not contribute to the accuracy of the solution. This was done by progressively increasing the mesh density of the coarse mesh and comparing the results from every mesh. When it was found that the increase in mesh density stops improving the solution, that mesh was chosen as the optimum mesh. The residuals obtained when using a coarse and a fine mesh are presented in Figs. 3.3, 3.4, 3.5 and 3.6.

Note that the residuals oscillate wildly when the coarse mesh was used (Fig. 3.3). This indicates that the mesh density is insufficient to resolve the solution domain. This also justifies the refinement of the mesh, in favor of a stable and accurate solution. The refined mesh is shown in Fig. 3.6. The corresponding residuals in Fig. 3.5 are well behaved, showing that the mesh density is sufficient.

The oscillating residuals are a result of "jumps" in the solution between the adjacent cells. These jumps originate in regions of large gradients, especially when the solution domain has not been resolved sufficiently. In order to avoid these jumps, the change in the solution between adjacent cells has to be kept at a minimum. This may be done by increasing the number of cells in those regions, so that now the adjacent cells are closer. This reduces the jumps in solutions and avoids instability.
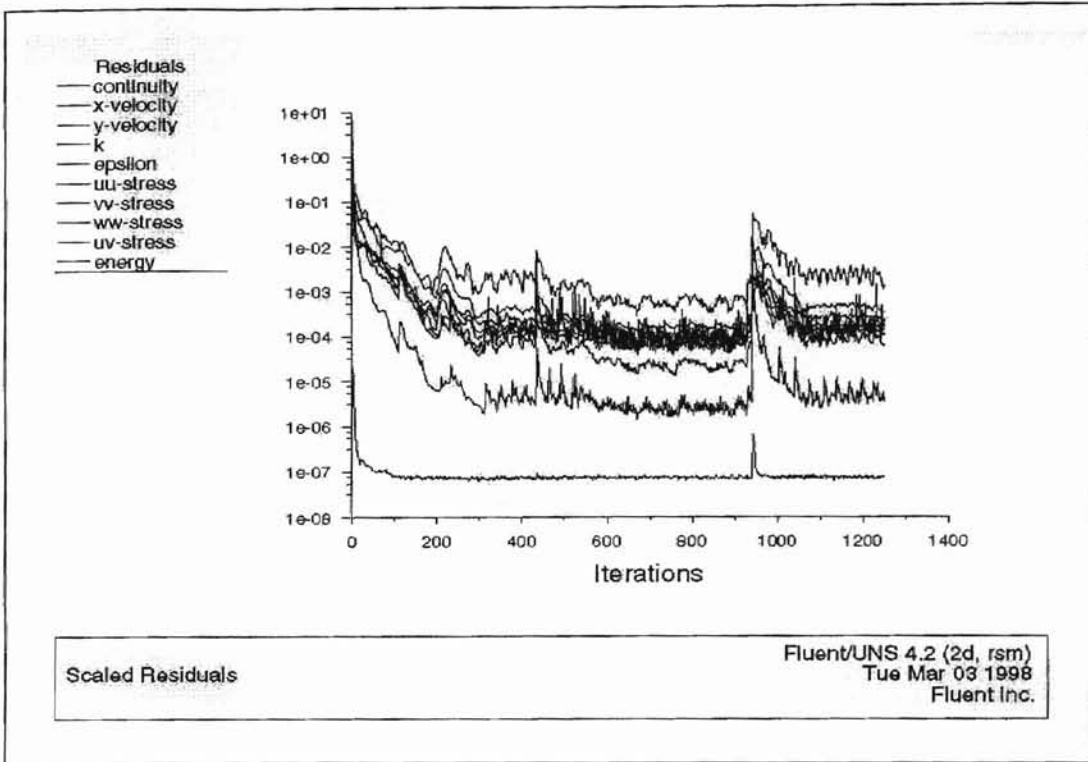
Figure 3.3 Residuals during calculation for the coarse mesh
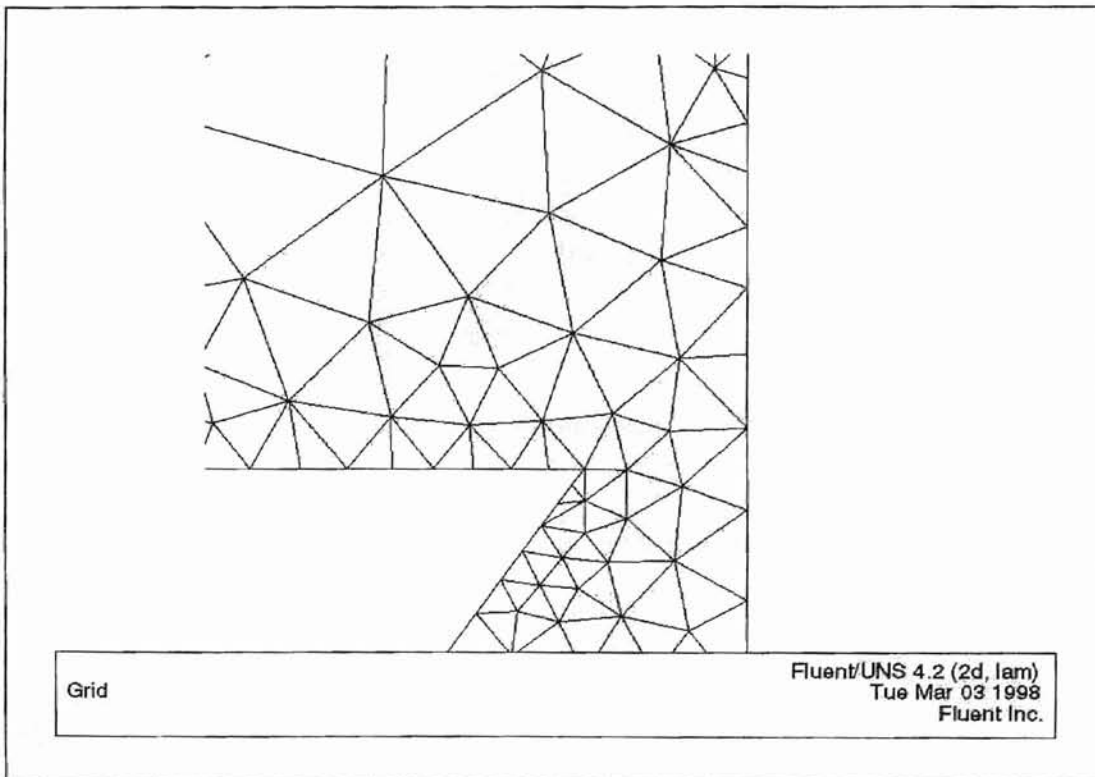
Figure 3.4 Close-up view of the nozzle region in the coarse mesh
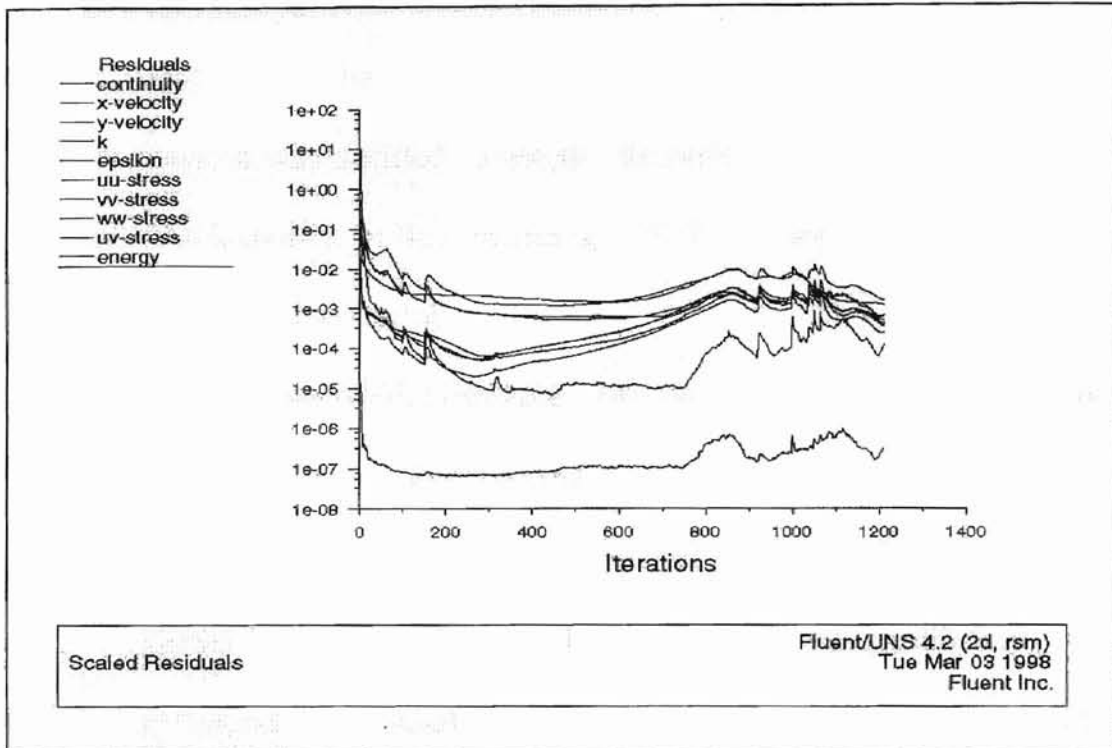
Figure 3.5 Residuals during calculation for the fine mesh
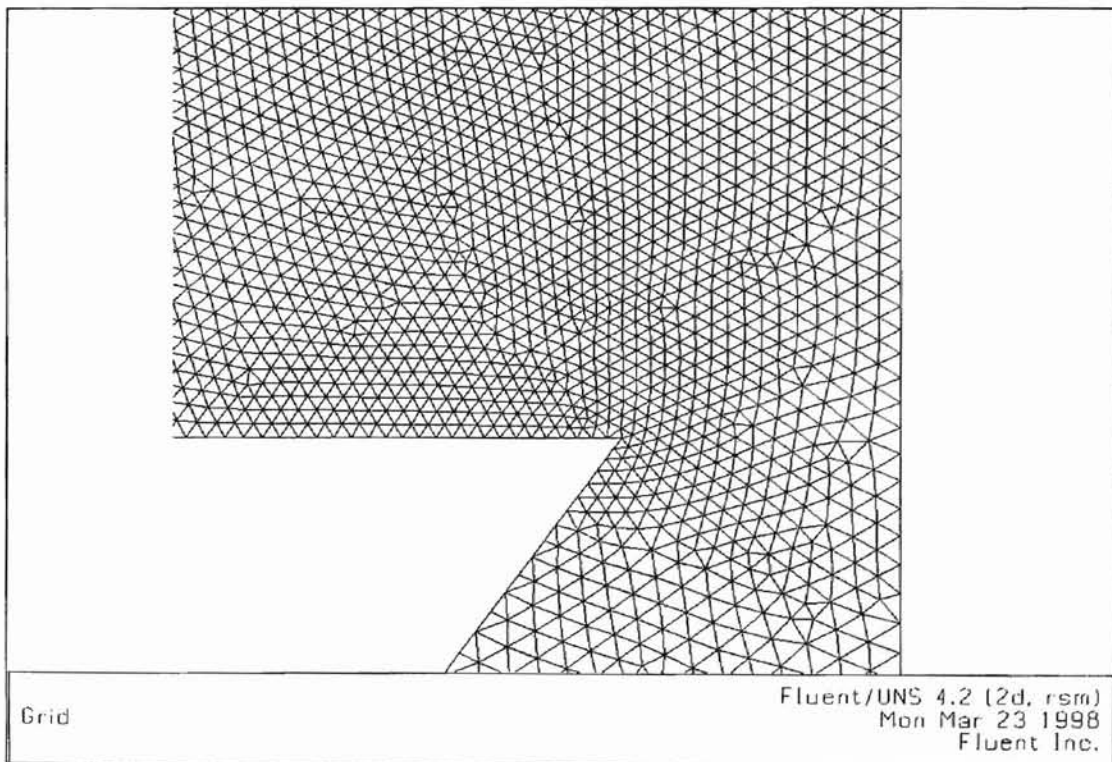
Figure 3.6 Close-up view of the nozzle region in the fine mesh

3.1.3 Justification of the turbulence model used

As described earlier, Fluent/UNS has different models for solving turbulent flows. It was decided to use the Reynolds Stress Model (RSM) for calculating the turbulent jet flow in this model. The reasons for choosing this model over the others are as follows:

- The Reynolds Stress Model can accurately model the flow separation and attachment better than any of the other models included in Fluent/UNS.

- RSM is found to be more accurate and reasonably fast when the near-wall flow treatment becomes critical. It uses the "Non-equilibrium wall function" approach to resolve the near-wall region. According to this method, the near wall region is considered to be divided into a viscous sublayer (layer closest to the wall, where laminar effects are dominating) and a fully turbulent layer. The non-equilibrium existing between these two layers is captured well by the RSM, which is crucial for accurate flow simulation. This approach has been recommended for situations involving wall bounded flows.

3.2 Solution Procedure

The solution procedure consists of applying a known supply pressure at the inlet, and solving for the various parameters over the entire solution domain. This process is repeated after changing different parameters, in order to study the effect of changing these parameters on the jet behavior.

Several interesting phenomena were observed during the solution process. For example, based on the initial value of pressure in the solution domain (i.e., cells), the rate of convergence was drastically affected. During the initial stages of calculation, the initial pressure was set as 0 psi throughout the entire domain. The calculations took about 4000 - 5000 iterations (and more than 15 hours) to achieve sufficient convergence. This was due to the fact that the propagation of the jet through the nozzle was very slow and hence it took a lot of time for the supply pressure to diffuse throughout the domain. When this problem was realized subsequent calculations were based on a non-zero initial pressure, usually set equal to the supply pressure. The new initial condition tremendously cut down the computing time, and solutions with the same level of convergence were now obtained within 1000 - 1500 iterations, taking less than 4 hours.

The under-relaxation parameters (factors used to diminish or magnify the change in the value of the solution variable after each step of calculation so as to improve stability of the solution or accelerate convergence) used during the calculations were found to exhibit an important behavior. Fluent/UNS has default values for these relaxation parameters set around 0.5 - 0.8. It was found that when the initial pressure in the solution domain was given as 0 psi, the under-relaxation parameters had to be changed to about 0.1. If this was not done, the solution was found to diverge. This low under-

relaxation factor also slows convergence. At the same time, when the initial pressure in the domain was made equal to the supply pressure, it was observed that the under-relaxation parameters could be maintained at the default values (0.5 - 0.8) without any oscillations or instability of the residuals. This greatly improves the rate of convergence. This phenomenon attributes to the drastic cutdown in the number of iterations when using an initialized pressure field at the beginning.

Initially, the supply pressure was set at a typical value, say 0.01 psi (69 Pa), and then the results were obtained and studied. If the jet was found to be separated, then the supply pressure was increased slightly, and the calculation process was repeated. This process was continued till the jet was found to attach. Thus to determine the threshold pressures calculations for several supply pressures had to be done as seen in Table 3.1. Typically, 5 - 6 different supply pressures were tested before deciding the critical pressures. The following table contains a particular case (R = 0.141", h = 0.1", b = 0.03", ρ = 0.0008") for which various supply pressures (in the same order as the calculations were done) were tested to find the critical pressures.

Table 3.1 Calculation procedure to find the critical pressures (R = 0.141", h = 0.1", b = 0.03", ρ = 0.0008")

Supply pressure, P		Behavior of Jet
psi	*N/m²*	*separated/attached*
0.010	69	separated
0.020	138	attached
0.015	103	attached
0.017	117	attached
0.013	*90*	*attached* *
0.014	97	attached
0.011	76	separated
0.012	*83*	*separated* **

* Upper critical pressure

** Lower critical pressure

3.3 Validity of the Computational Model

After all the above considerations were incorporated into building the model and a few solutions were obtained, the model needed to be validated. This was made possible by the availability of experimental results of Aravamudhan (1998). The validation was done by comparing the jet behavior predicted by the computational model with the behavior observed experimentally for the same test conditions. Qualitative observations indicated that the model was able to predict the existence of three different regions : separated, attached, and bistable region (Fig. 3.11).

Initially the compressibility of air was not taken into consideration during the solution process. When the results were obtained, it was found

that the maximum velocity in the flow field was close to 0.3 times the speed of sound. Hence, it was decided to consider the effects of compressibility of air. When the effects of compressibility of air was considered, the solutions were found to be comparable to Aravamudhan's (1998) experimental results.

3.4 Results

3.4.1 Effect of supply pressure of air

The first parameter whose effect on the jet behavior was tested was the supply pressure of air. It was known experimentally (Aravamudhan, 1998) that with all other parameters kept constant, an increasing supply pressure tends to result in an attached jet and decreasing supply pressure a separated jet. A computational model was built with R = 0.141", b = 0.03" and h = 0", and was subjected to supply pressures ranging from 0.1 psi (690 Pa) to 0.15 psi (1035 Pa). Each time the pressure value over the entire domain was initialized with the supply pressure value. As discussed earlier, this was found to increase the rate of convergence, and thus reduce the time needed for getting a converged solution.

We can define the critical supply pressures as follows. The *Lower critical pressure P$_1$* is a supply pressure below which the jet is always separated. The *Upper critical pressure P$_2$*, is a supply pressure above which the jet is always attached to the adjacent surface. When the supply pressure is in

between these two critical pressures, the jet exhibits a *bistable* condition. In this bistable region, the jet can remain either attached or separated, depending on external disturbances.

To disturb the jet computationally and hence study the bistable nature of the jet, the initial value of the x-velocity over the entire domain was given as either 0 m/s or 1 m/s. When the initial x-velocity is given as 1 m/s, the situation is similar to one in which the air jet is forced to be attached to the wall. If that supply pressure was not in the bistable zone (say P = 0.10 psi in the above case), then the air jet was seen to separate even with the initial x-velocity = 1 m/s. This was repeated for every supply pressure. The results obtained have been tabulated in Table 3.2.

Table 3.2 Effect of supply pressure on jet behavior
(R = 0.141", b = 0.03",h = 0")

Supply pressure, P		Initial x-velocity	Behavior of Jet
psi	*Pa*	*m/s*	*separated/attached*
0.10	69	0	Separated
0.10	69	1	Separated
0.13	345	0	Separated
0.13	345	1	Attached
0.15	552	0	Attached
0.15	552	1	Attached

Figures 3.7 and 3.8 show the velocity contours plots at P = 0.1 psi (690 Pa) and P = 0.15 psi (1035 Pa), respectively. Jet separation and attachment can

be clearly seen from those figures and are indicative of the method used for deciding whether a particular flow was attached or separated.

However, the jet was seen to have different attachment and separation properties at different supply pressures. If we look at Fig. 3.9, we may find that the jet is attached to the surface for a small distance before it separates. Figure 3.10 shows an attached jet ($R = 0.141"$, $b = 0.02"$, $h = 0.1"$, $P = 0.005$ psi), which is slightly different from Fig. 3.8 (also showing an attached jet) because the jet separates from the surface at the end of the curvature, only to reattach at the downstream.
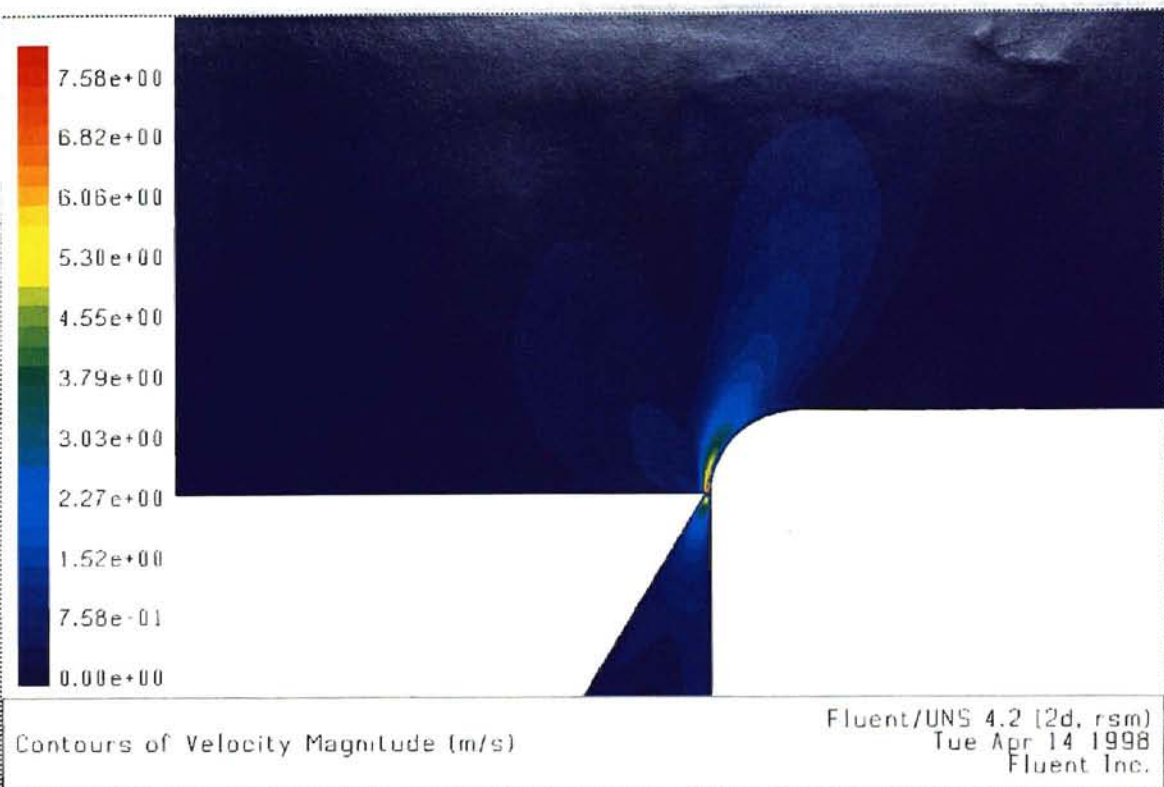
Figure 3.7 Contours of velocity magnitude showing jet separation (b = 0.03", R = 0.141", h = 0", P = 0.10 psi)

Figure 3.8 Contours of velocity magnitude showing jet attachment (b = 0.03", R = 0.141", h = 0", P = 0.15 psi)
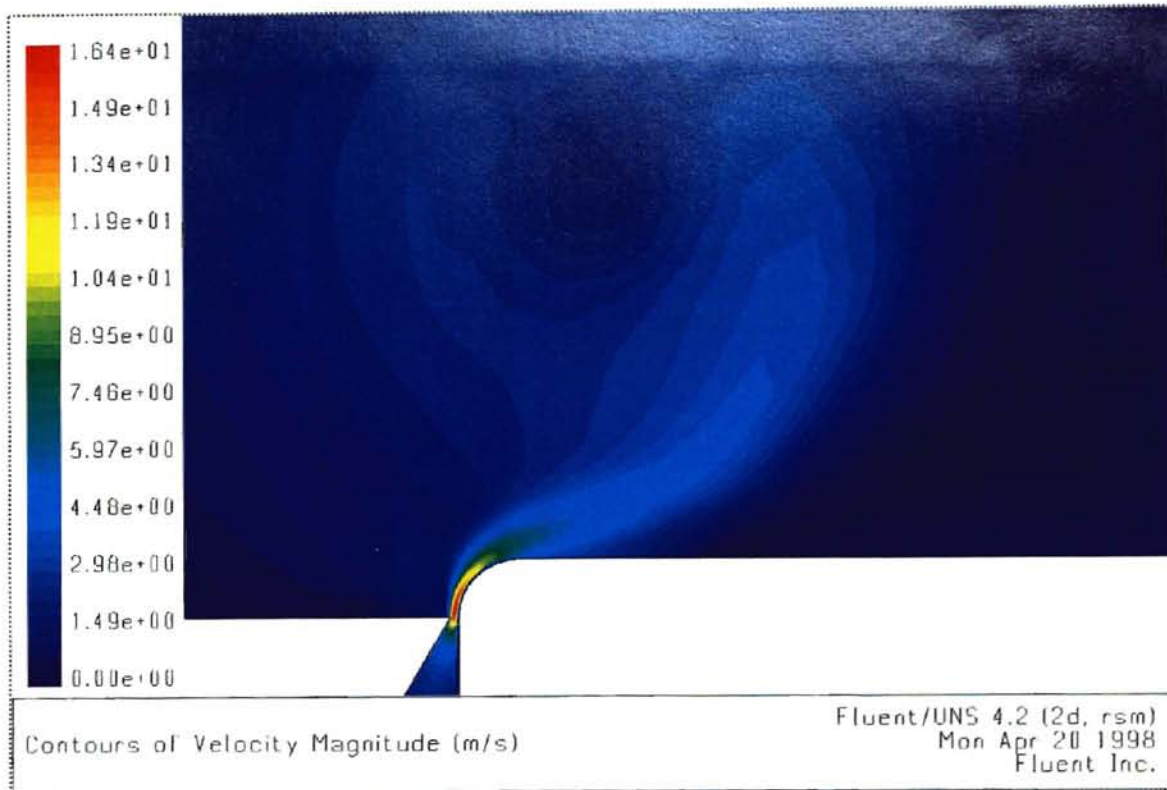
Figure 3.9 Contours of velocity magnitude showing flow separation after a
certain distance (R = 0.141", b = 0.02", h = 0", P = 0.03 psi)
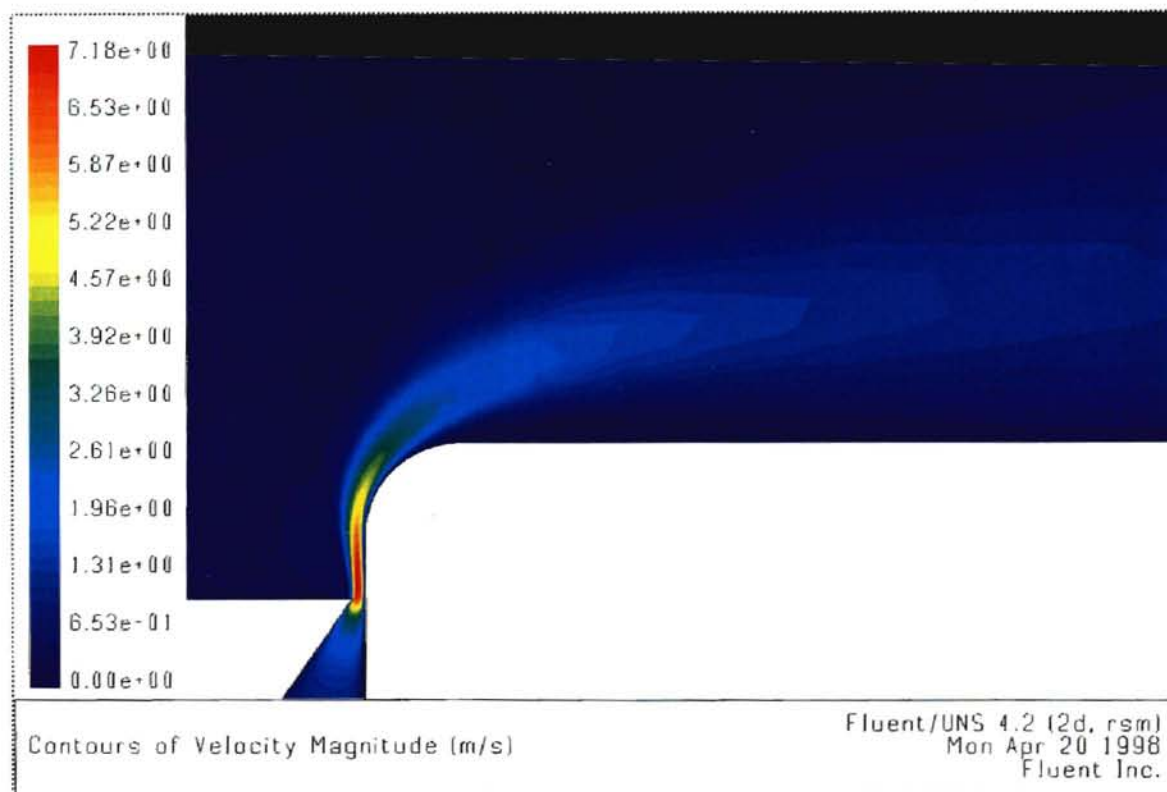
Figure 3.10 Contours of velocity magnitude showing jet attachment after
a local separation (R = 0.141", b = 0.02", h = 0.1", P = 0.005 psi)

From the above data, we find that the supply pressure has a significant effect on the jet behavior. When the pressure was increased from 0.1 psi to 0.15 psi, the jet changed from a separated jet to an attached jet, exhibiting a bistable condition in between.

We can also see that this influence of supply pressure on the jet behavior is consistent and unchanged, regardless of other parameters like nozzle offset. When the nozzle offset varies between 0″ and 0.15″ the behavior of the jet with respect to change in supply pressure remains the same, i.e., as the supply pressure increases from 0 psi to a higher value, the jet
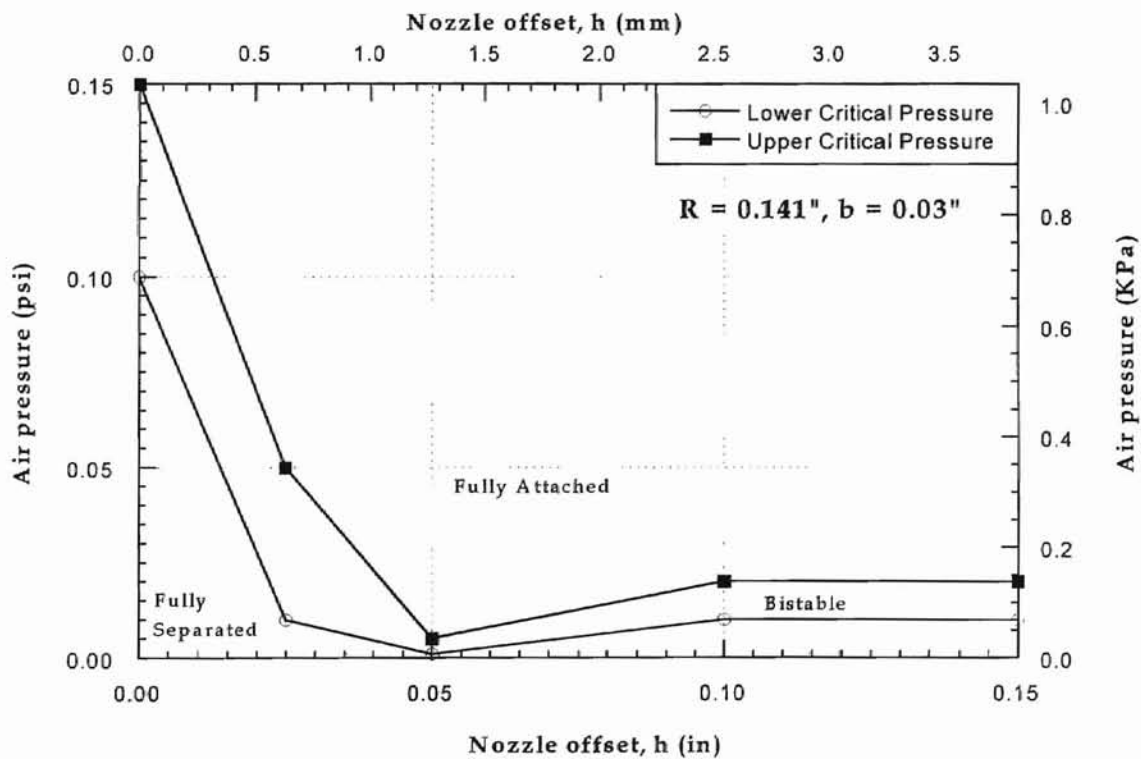
Figure 3.11 Effect of supply pressure on jet behavior

remains separated till the lower critical pressure is reached, after which it exhibits a bistable behavior. When the supply pressure is increased further, the jet becomes fully attached after the upper critical pressure is reached. Figure 3.11 ascertains this point.

3.4.2 Effect of surface roughness

Surface roughness was also found to affect the jet characteristics in a significant way. The study model used had the following dimensions : R = 0.141", h = 0.1", and b = 0.03". The solutions were obtained for several supply pressures at the inlet to establish the attachment/separation criteria as affected by the surface roughness. Various values of surface roughness ranging from 0 mm (corresponding to smooth walls) to 0.4 mm (approximately half the nozzle width for this configuration) were tested. The results are tabulated below.

Table 3.3 Effect of surface roughness (R = 0.141", b = 0.03", h = 0.1")

Surface Roughness, ρ		Lower Critical Pressure, P_1		Upper Critical pressure, P_2	
inches	mm	psi	Pa	psi	Pa
0	0	0.013	89.6	0.015	103.4
7.874×10^{-4}	0.02	0.012	82.7	0.013	89.65
7.874×10^{-3}	0.2	0.01	68.9	0.011	75.85
1.181×10^{-2}	0.3	0.006	41.3	0.008	55.17
1.575×10^{-2}	0.4	0.004	27.6	0.006	41.38

The change of surface roughness was found to have a favorable impact on the jet characteristics, in that it increased adherence of the jet to the wall.

As the surface roughness is increased, the upper critical pressure required for attachment of the jet goes down.
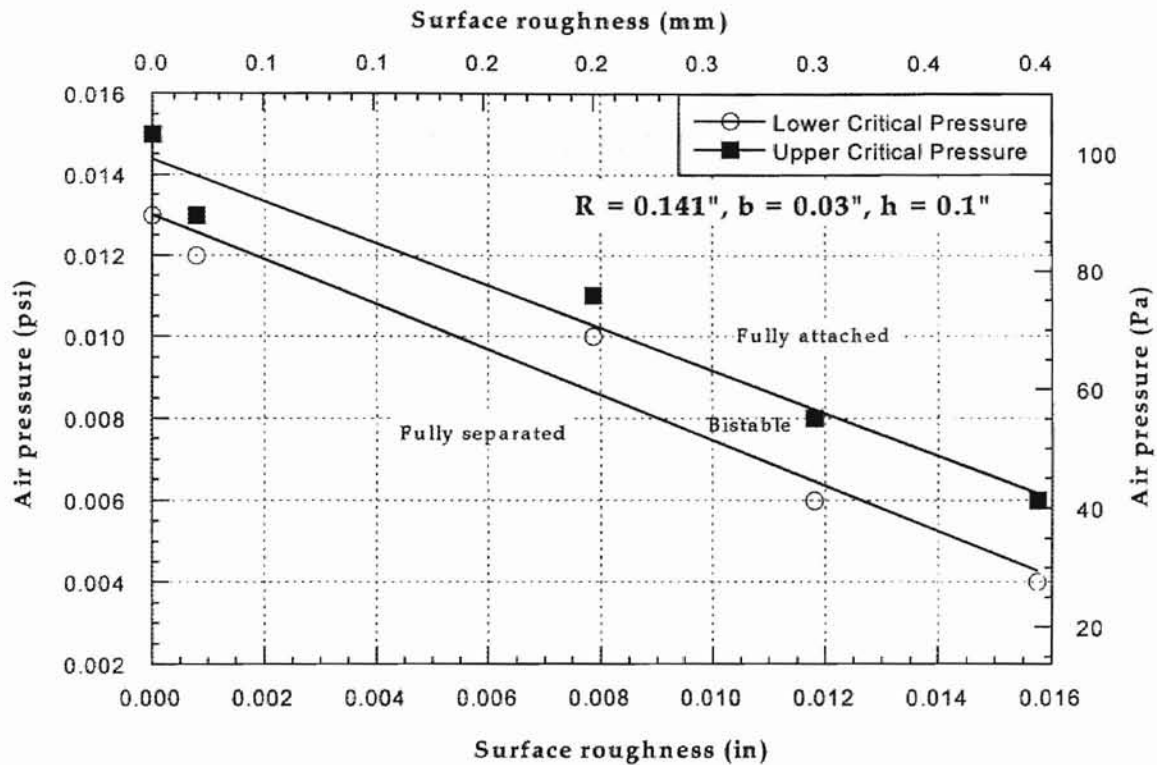
Figure 3.12 Effect of surface roughness on jet characteristics (R = 0.141", b = 0.03", h = 0.1")

Note that Fig. 3.12 indicates both the upper and lower critical pressures. As the surface roughness is increased, both the lower and upper critical pressures can be seen to decrease. This downward trend means that the increase in surface roughness helps the jet attach to the surface. This is found to be in accordance with Reba (1966) who demonstrated that a grooved adjacent surface improves attachment of the Coanda air jet, and Zhang and

31

Ko (1996) who showed that the grooves on a cylinder result in better reattachment of the jet.

3.4.3 Effect of nozzle width

Nozzle width, b (Fig. 3.2) was another important parameter that was studied subsequently. Several models were built with varying nozzle widths, keeping the radius of curvature constant at R = 0.141" (3.571 mm). Then each model was subjected to a large number of supply pressures, and solutions were calculated. Hence the jet attachment/separation criteria was established as a function of nozzle width, b. The computational experiments were repeated for various values of nozzle offset. This enabled the investigation of the effect of changing nozzle width for various nozzle offsets. The results have been tabulated below.

Table 3.4 Effect of nozzle width (R = 0.141")

R = 0.141" (3.571 mm), b = 0.02" (0.508 mm)

Nozzle Offset, h		Lower Critical Pressure, P_1^*		Upper Critical pressure, P_2^*	
inches	mm	psi	Pa	psi	Pa
0	0	0.05	344.8	0.06	413.76
0.025	0.635	0.006	41.38	0.01	68.96
0.05	1.27	0.008	55.17	0.01	68.96
0.1	2.54	0.01	68.96	0.03	206.88
0.15	3.81	0.005	34.48	0.006	41.38

R = 0.141" (3.571 mm), b = 0.03" (0.762 mm)

Nozzle Offset, h		Lower Critical Pressure, P_1 *		Upper Critical pressure, P_2 *	
inches	mm	psi	Pa	psi	Pa
0	0	0.1	689.6	0.15	1034.4
0.025	0.635	0.01	68.96	0.05	344.8
0.05	1.27	0.001	6.896	0.005	34.48
0.1	2.54	0.01	68.96	0.02	137.92
0.15	3.81	0.01	68.96	0.02	137.92

R = 0.141" (3.571 mm), b = 0.04" (1.016 mm)

Nozzle Offset, h		Lower Critical Pressure, P_1 *		Upper Critical pressure, P_2 *	
inches	mm	psi	Pa	psi	Pa
0	0	0.3	2068.8	0.4	2758.4
0.025	0.635	0.02	137.92	0.05	344.8
0.05	1.27	0.01	68.96	0.05	344.8
0.1	2.54	0.005	34.48	0.01	68.96

* The data shown in Table 3.4 is not a complete set of data. A certain degree of uncertainty does exist in the classification of data, as the separation and attachment criteria were not tested for a wide range of pressures due to time constraint.
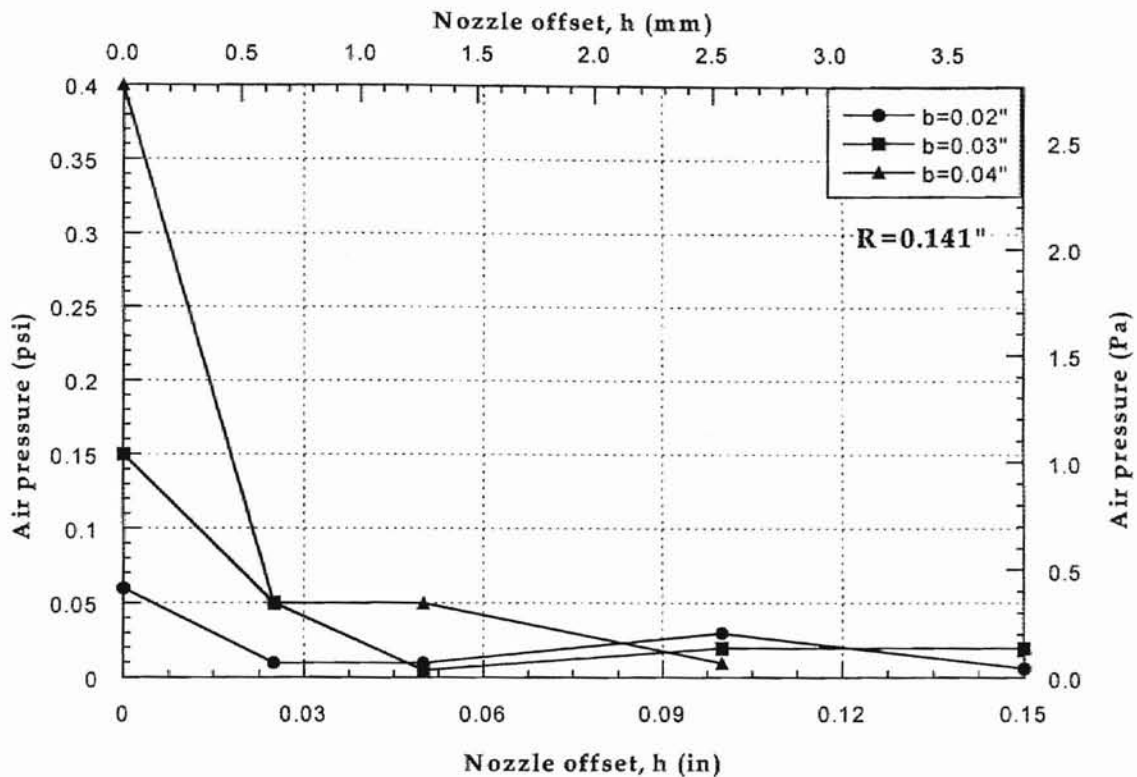
Figure 3.13 Effect of nozzle width (R = 0.141")

It should be mentioned that the above graph has a certain degree of uncertainty as the separation and attachment criteria could not be tested over a wide range of pressures due to time constraint. Note that Fig. 3.13 shows only the upper critical pressure curves for b = 0.02", 0.03" and 0.04". It shows that the nozzle width has a large impact at low h values. In other words, the nozzle width seems to have a significant influence on the jet behavior only for small values of h. As the value of h goes above 0.05" (1.27 mm), all the curves seem to flatten out and collapse to almost the same pressure region. Hence it may be noted that values of h between 0.05" and 0.15" are preferred, as the upper critical pressure is low and almost independent of the nozzle width.

This means that at these values of h, a low supply pressure is sufficient to keep the jet attached to the curved surface.

If we look at the velocity magnitude contour plots (Figs. 3.14 and 3.15), we see that as the nozzle width increases from 0.02" (0.508 mm) to 0.03" (0.762 mm), keeping all other parameters constant, the jet diffuses more rapidly for a larger nozzle width. This effect was seen to be more pronounced at lower h values. This might be the reason for the corresponding rapid increase in the upper critical pressure. We may also note that more amount of air is entrained into the mainstream when the nozzle width is larger. It was also noted that the jet stayed as a thin jet (i.e. did not diffuse very much) at higher pressures but was susceptible to rapid diffusion at lower supply pressures.
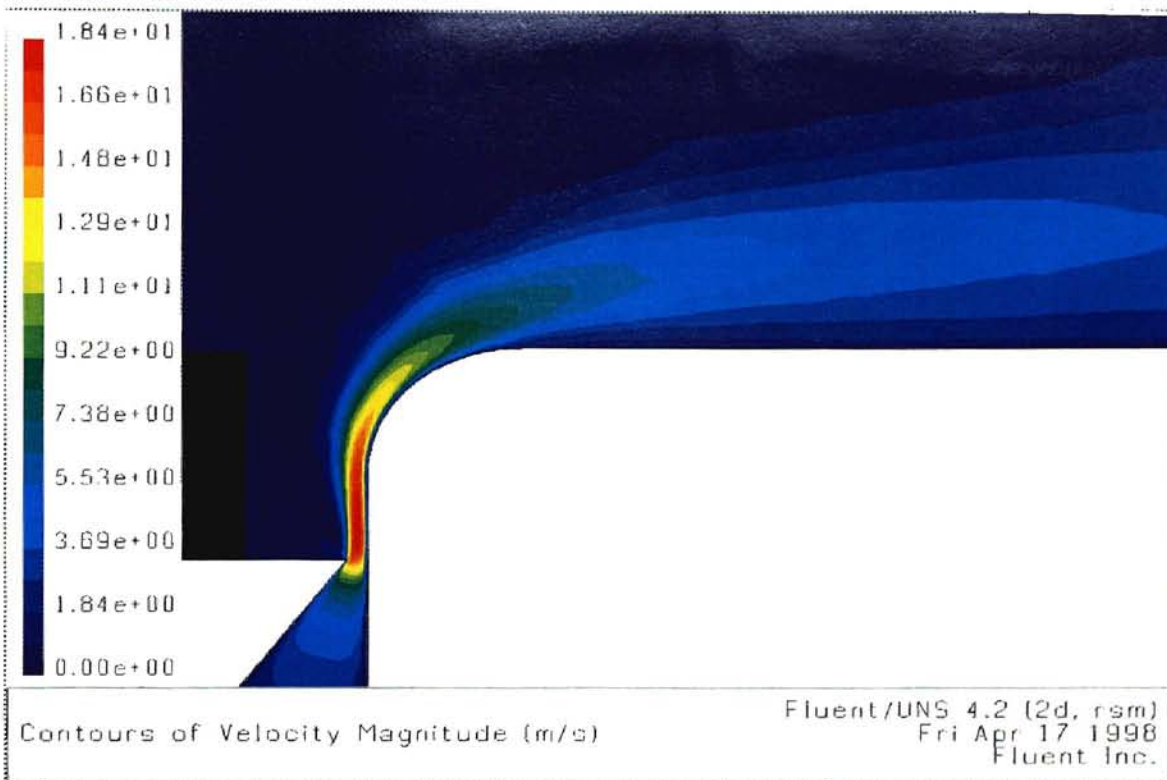
Figure 3.14 Contours of velocity magnitude showing jet diffusion
(R = 0.141″, b = 0.02″, h = 0.1″, P = 0.03 psi)
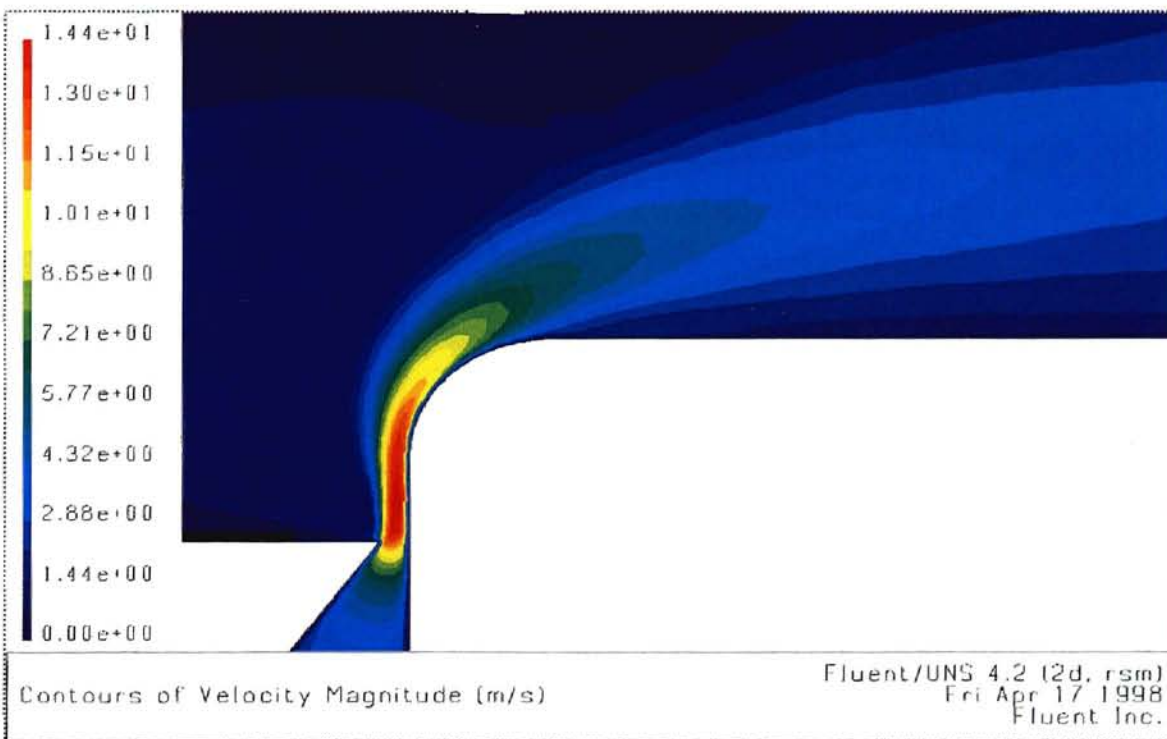
Figure 3.15 Contours of velocity magnitude showing increased jet diffusion
(R = 0.141″, b = 0.03″, h = 0.1″, P = 0.03 psi)

Contours of Velocity Magnitude (m/s)
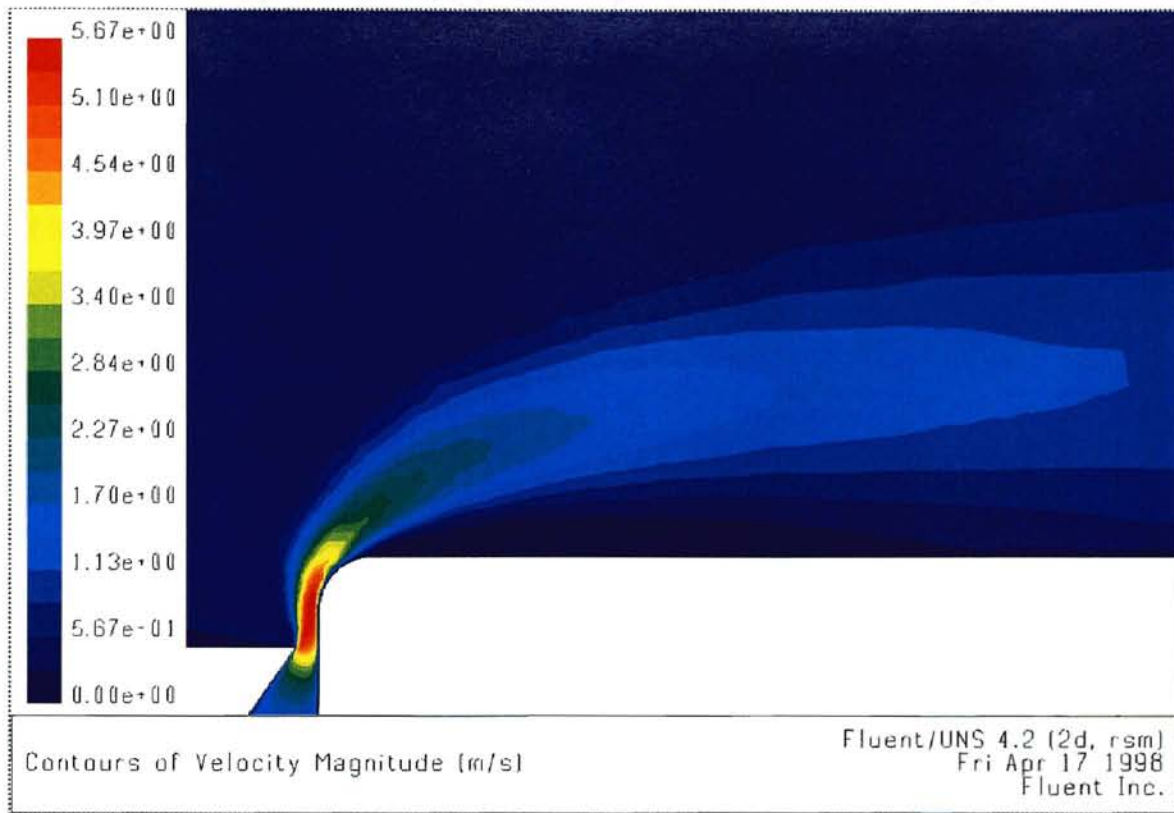
Figure 3.16 Contours of velocity magnitude showing recirculation
(R = 0.141″, b = 0.06″, P = 0.003 psi)

Another interesting phenomenon was that at higher values of b (b =

0.06″), there existed a recirculation zone between the mainstream and the

adjacent surface as seen in Fig. 3.16. In that recirculation zone, the flow

velocities were nearly zero and it existed throughout the entire length of the

domain. The jet was also found to "float" close to the surface without explicit

separation or attachment. It might also be seen that the jet width increases

very rapidly as the nozzle width is quite high.

3.4.4 Effect of nozzle offset

The next step was to analyze the effect of nozzle offset, h (Fig. 3.2) on the behavior of air jet. The radius of curvature was fixed at R = 0.141" (3.571 mm). Several models were created by varying the value of h between 0.0" and 0.1" (2.54 mm). The supply pressure was varied to find out the jet separation/attachment criteria. The results are tabulated below in Table 3.5. We find that the change in the nozzle offset from 0.0" to 0.1" (2.54 mm) results in a dramatic change in the jet attachment/separation properties.

Table 3.5 Effect of nozzle offset (R = 0.141")

R = 0.141" (3.571 mm), h = 0"

Nozzle width, b		Lower Critical Pressure, P_1		Upper Critical pressure, P_2	
inches	mm	psi	Pa	psi	Pa
0.01	0.254	0.05	344.8	0.1	689.6
0.02	0.508	0.05	344.8	0.06	413.8
0.03	0.762	0.1	689.6	0.15	1034.4
0.04	1.016	0.3	2068.8	0.4	2758.4

R = 0.141" (3.571 mm), h = 0.05" (1.27 mm)

Nozzle width, b		Lower Critical Pressure, P_1		Upper Critical pressure, P_2	
inches	mm	psi	Pa	psi	Pa
0.02	0.508	0.008	55.17	0.01	68.96
0.03	0.762	0.001	6.9	0.005	34.48
0.04	1.016	0.01	68.96	0.05	344.8
0.05	1.27	0.07	482.72	0.08	551.68
0.06	1.524	0.05	344.8	0.1	689.6

R = 0.141" (3.571 mm), h = 0.1" (2.54 mm)

Nozzle width, b		Lower Critical Pressure, P_1		Upper Critical pressure, P_2	
inches	mm	psi	Pa	psi	Pa
0.03	0.762	0.01	68.96	0.02	139.22
0.04	1.016	0.005	34.48	0.01	68.96
0.05	1.27	0.005	34.48	0.008	55.17
0.06	1.524	0.003	20.69	0.005	34.48
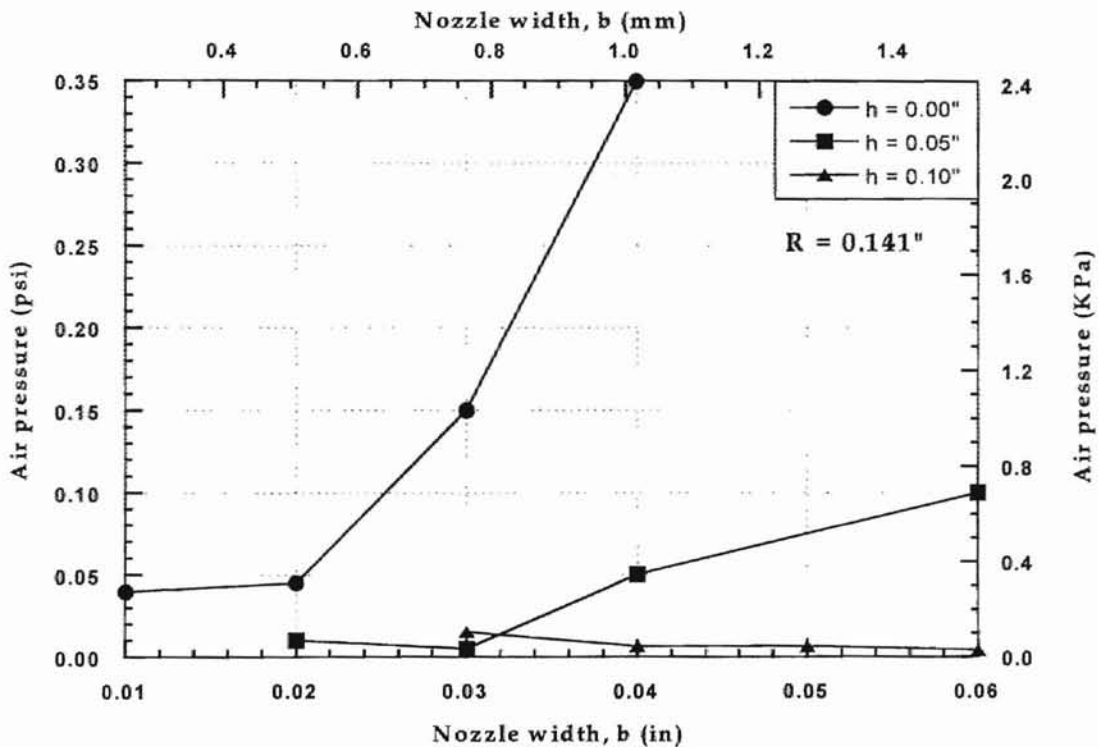
Figure 3.17 Effect of nozzle offset on the upper critical pressure (R = 0.141")

From Fig. 3.17, it is seen that when h = 0", the upper critical pressure curve is quite high. As h increases towards 0.1", we find that the upper critical pressure shows a downward trend, which becomes very clear at h = 0.1". This drastic behavior of the jet, with respect to increase in h, needs to be

kept in mind when designing air floatation devices. This situation could be used advantageously by designing the air floatation devices to have h = 0.1" (2.54 mm), so that the jet is fully attached even at low supply pressures. From our definition of h (Fig. 3.2), it may be noted that h can also have negative values.

We have considered the effect of several parameters upon the jet behavior separately. Now, if we consider the effect of nozzle width and nozzle offset together, we find that the effect of one depends on the other. For example, from Figs. 3.13 and 3.17, we may find that as h changes from 0" to 0.1", its effect on the upper critical pressure is pronounced only when the b value is greater than 0.02" (0.508 mm). When the nozzle width is less than 0.02", the change of h from 0" to 0.1" does not cause any drastic change in the critical pressure.

Similarly, the change of jet behavior with respect to change in b is drastic only when the h value is between 0" and 0.05" . Beyond this range of h, the upper critical pressures flatten out and become independent of the nozzle width. It was also found that when b is large, jet diffusion occurs more rapidly. The jet stream entrains more air and it becomes more difficult for the jet to fully attach to the surface. In such situations, higher supply pressures are required for full attachment.

Hence from these observations, it becomes apparent that when designing and operating an air floatation device, not only the individual parameters need to be considered, but their combined configurations must also be considered and optimized.

CHAPTER 4
COMPUTATIONAL MODELING OF THE INTERACTION BETWEEN THE COANDA AIR JET AND A WEB

After the effects of various parameters on the free jet behavior were studied, it was decided to extend the model to include the effects of a stationary rigid web placed as shown in Fig. 4.1. The pressure distribution on the web surface and the aerodynamic friction force exerted by the jet upon the web were the key parameters to be studied using this model. The model approximately simulates a situation in which the Coanda air jet is used for generating the aerodynamic traction in the machine or cross direction. Note that Figs. 4.1 and 4.2 are not to scale.
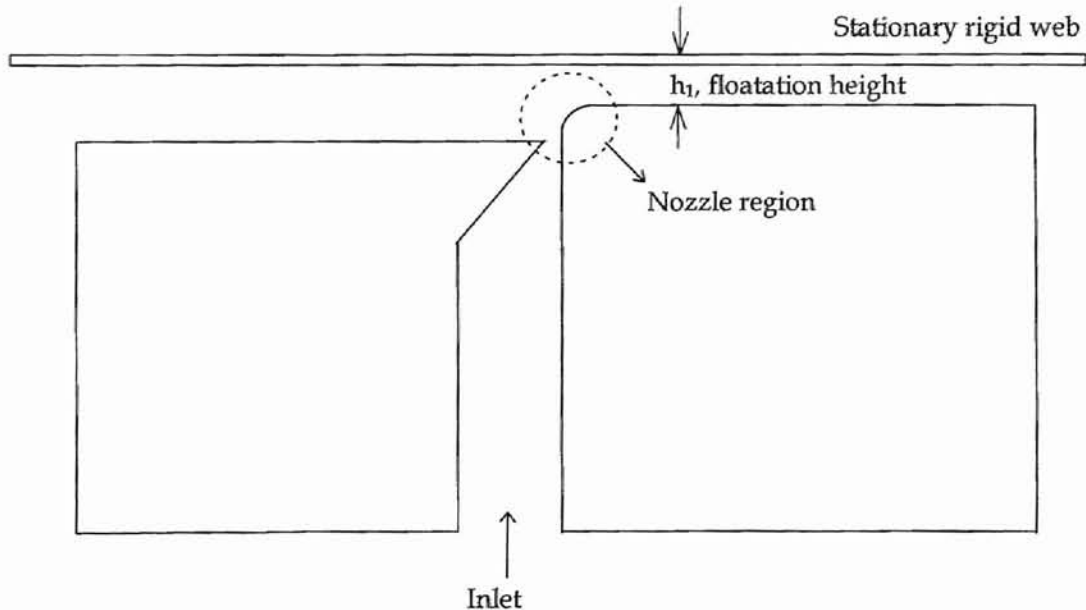
Figure 4.1 Schematic of the model which includes a stationary rigid web

4.1 Stationary Rigid Web

The computational model of this physical situation was created using techniques described earlier. This model is more complicated because describing the jet outlet is more involved in this case due to the presence of the web. The computational domain is shown in Fig. 4.2. We see that the floatation region between the web and the wall has to be described by a dense mesh, because of the high velocities and pressure changes intuitively expected. Since we define the exits as pressure outlet boundaries which are maintained at constant atmospheric pressure, care should be taken not to place a constraint on the jet. The exits (pressure outlet boundaries) were therefore placed as far as possible from the nozzle. This tends to increase the domain size without contributing much to the solution. Hence the two considerations should be wisely balanced .
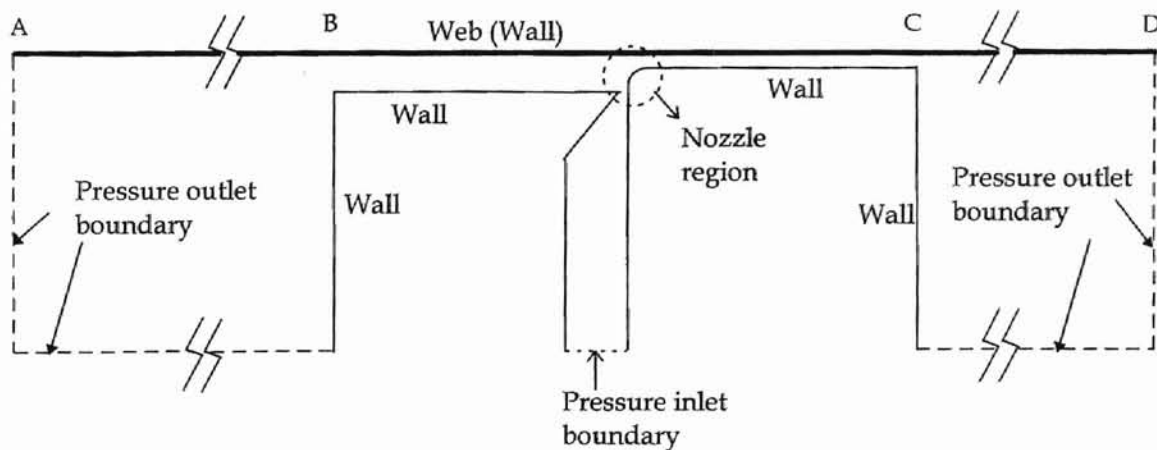
Figure 4.2 Computational model of the physical situation

The two box-like regions on the left and right sides of the nozzle region are present to provide adequate space for the jet to diffuse and hence to avoid any constraints on the jet behavior.

The stationary rigid web was described by a wall with zero surface roughness. The inherent limitation in Fluent/UNS, as to the maximum number of nodes that can be used to describe a single edge is 240. Initially the web was modeled using a single edge, AD. As can be seen from Fig. 4.2, the web represents a very long boundary spanning the full length of the model, and hence 240 nodes were not enough for describing the mesh boundary accurately. So, it was decided to describe the web using 3 edges (AB, BC and CD) instead of 1. Since we now have 3 edges representing the web, the maximum number of nodes that may be used to resolve the web is 720, which is more than sufficient.

As it was anticipated that the solution might oscillate due to large gradients during iterations before it reaches a stable condition, it was decided to pay special attention to the local mesh density. The nozzle region has large gradients of the air pressure and flow velocity. If the region is resolved using only a few cells, the solution jumps in steps between adjacent cells causing the solution to oscillate and diverge. The near wall region also has large gradients because of the no-slip condition being enforced at the wall. This results in a sharp velocity profile close to the wall, which needs to be described by a large

number of cells to avoid any instability.

To begin with, a simple mesh (with no near-wall and nozzle region mesh density variation) was generated to describe the whole region (Fig. 4.3). and the solution was obtained for a supply pressure of 8 inches of water. An initial pressure value of 8 inches of water was given for the entire solution domain, as this was found to accelerate convergence during the calculations of Coanda air jet in free space. It was found that this initial value for pressure did help in convergence by accelerating the diffusion of the jet through the floatation region.

Grid

Fluent/UNS 4.2 (2d. lam)
Sat Mar 21 1998
Fluent Inc.
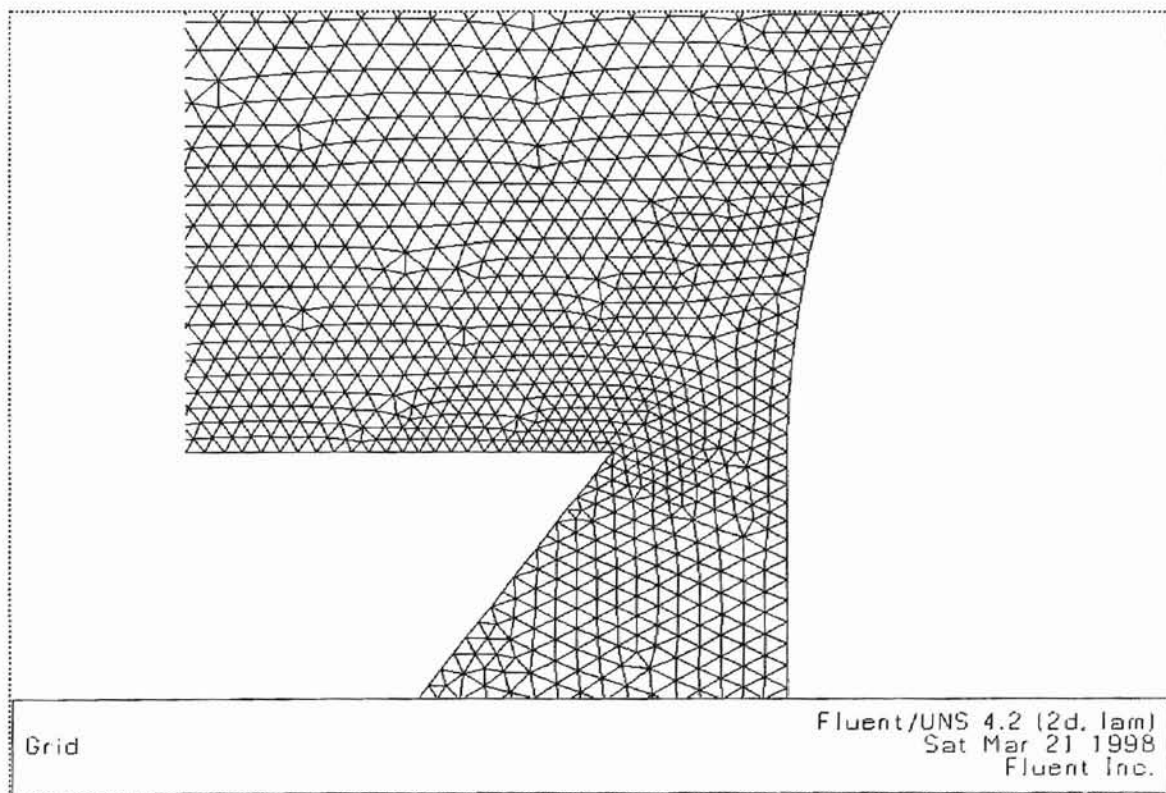
Figure 4.3 Simple mesh used in the beginning of calculations

The intermediate solutions obtained showed that there is a high

pressure gradient flow near the nozzle and in the floatation region. Thus it became clear that the mesh had to be locally refined to improve the credibility of the model. So, the mesh was "adapted" using the gradient adaption feature in Fluent/UNS. Mesh adaption is an in-built feature of Fluent/UNS, by which the automatic local refinement of the mesh is made possible by increasing the mesh density in those regions where the gradient of the solution is above a specified upper limit. The cells are broken into two or more cells, so that the gradient between adjacent cells is within the specified upper limit.

This feature also permits the coarsening of the mesh in those regions where the grid is excessively dense when compared to the gradients of the solution in that region, by specifying a lower limit for the gradients. Two or more cells are merged together such that the gradient between adjacent cells becomes above the lower limit specified.

When the simple mesh was adapted using the solution obtained, the nozzle region was automatically identified as a high gradient zone and was refined. But in the near wall regions, the mesh still remained coarse. This might have been due to the fact that the initial mesh was too coarse to capture the effect of no-slip (and hence zero-velocity) at the walls. Hence, the "Boundary adaption" feature of Fluent/UNS was used to refine the near wall region. This feature can be used to multiply the number of cells within a

certain distance from any given boundary by a given factor. This results in a near wall mesh refinement as seen in Fig. 4.4.
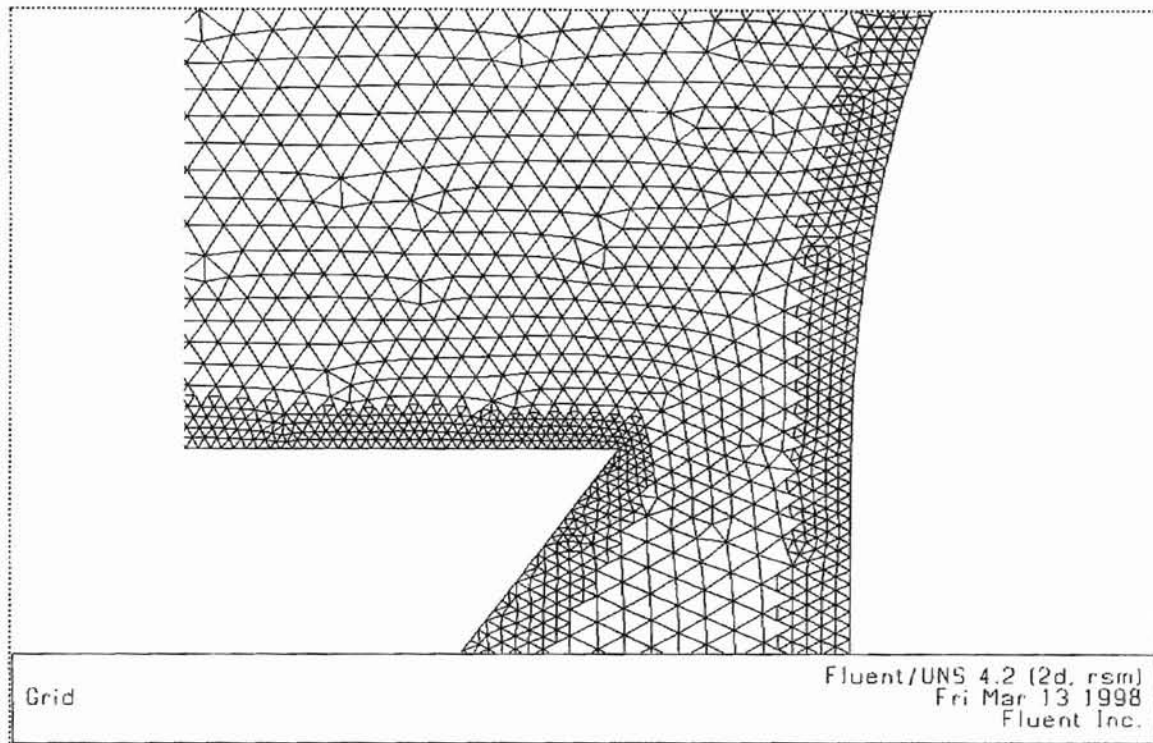
Figure 4.4 Varying mesh density in the nozzle region

One important factor to be considered at this point, is the increase in the number of cells as a result of mesh refinement. Care should be taken when using these automatic refinement features of Fluent/UNS, as they tend to increase the mesh size tremendously which will eventually increase the memory requirements and decrease the calculation speed.

It might be noted that in this case ($R = 0.172'''$, $b = 0.025''$, $h = 0''$, $h_1 = 0.15''$), the mesh refinement did not seem to affect the computing speed

adversely. It might be due to the reason that the simple mesh we had started with was very coarse, and subsequent refinement only brought it to an optimum. The solution residuals were highly oscillating with the simple mesh, but became more stable as a result of the mesh refinement. The final refined mesh (Fig. 4.4) contained about 30,000 nodes.

This mesh was eventually used to calculate the various parameter profiles along the web. The supply pressure was set at values of 8, 12 and 16 inches of water. The solution domain was initialized appropriately (with the supply pressure) and the solutions were obtained. The solution convergence took about 3000 - 4000 iterations for a residual convergence monitor of 1E-05. A "residual convergence monitor" is a value in Fluent/UNS that the residuals are checked against to see if convergence has reached or not. This is a relative, non-dimensional value which is compared against the normalized residuals. Residuals are normalized by dividing by the maximum residual calculated until that iteration. This ensures that the residuals are always in $O(1)$. When the sum of the normalized residuals becomes smaller than the monitor value, the solution is said to be converged.

4.2 Results and Discussion

4.2.1 Pressure distribution

If we look at the pressure distribution on the web for different supply pressures (Fig. 4.5), we find that the pressure drops to below atmospheric upstream of the nozzle region (x < 0″) resulting in the entrainment of air. If we take a closer look at the trends of these curves, we can find dips in the pressure profiles near the nozzle (-0.5″ < x < 0.5″).
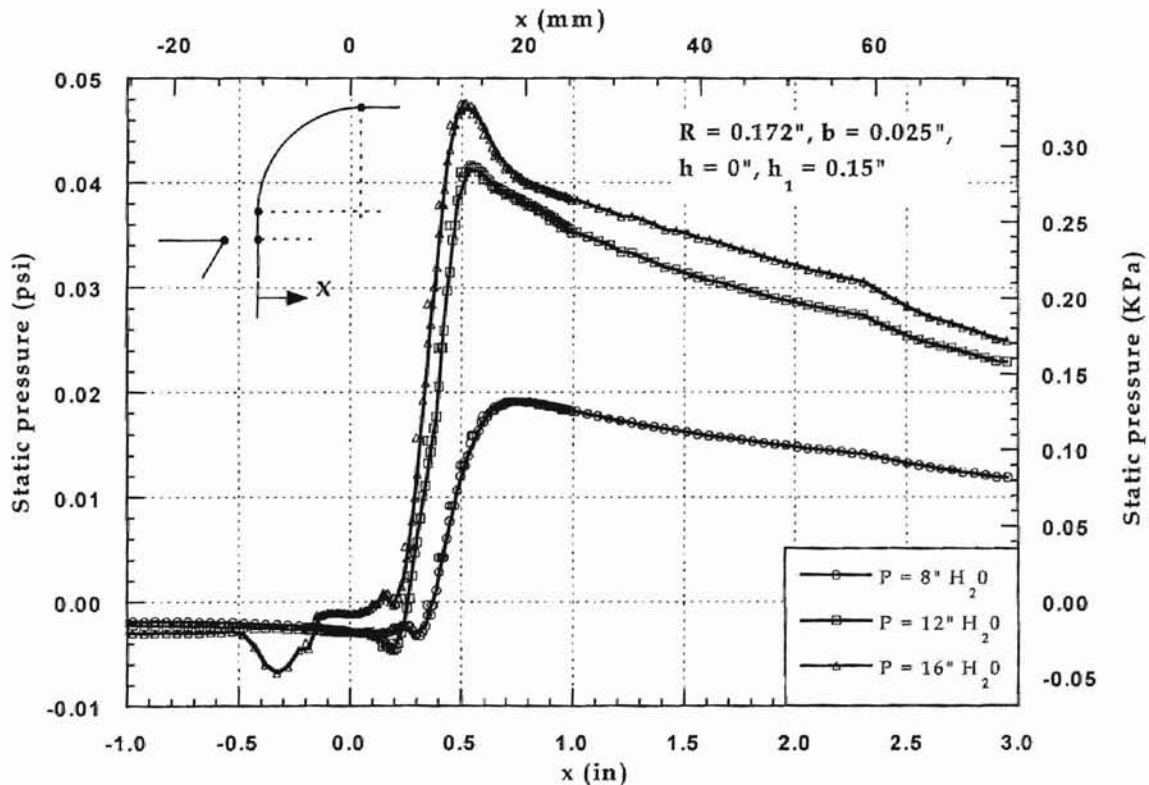
Figure 4.5 Pressure distribution on the stationary rigid web

Figure 4.6 gives a close-up of the pressure distribution near the nozzle region. Comparing the profiles at different supply pressures, we see that this dip shifts to the left as the supply pressure is increased. One other thing we might note here is that the change in magnitude of the pressure peaks is not proportional to the supply pressure. The pressure peaks seem to increase at a slower rate. This mean that there might exist an upper supply pressure value beyond which the increase in supply pressure might not contribute much to the pressure on the web.
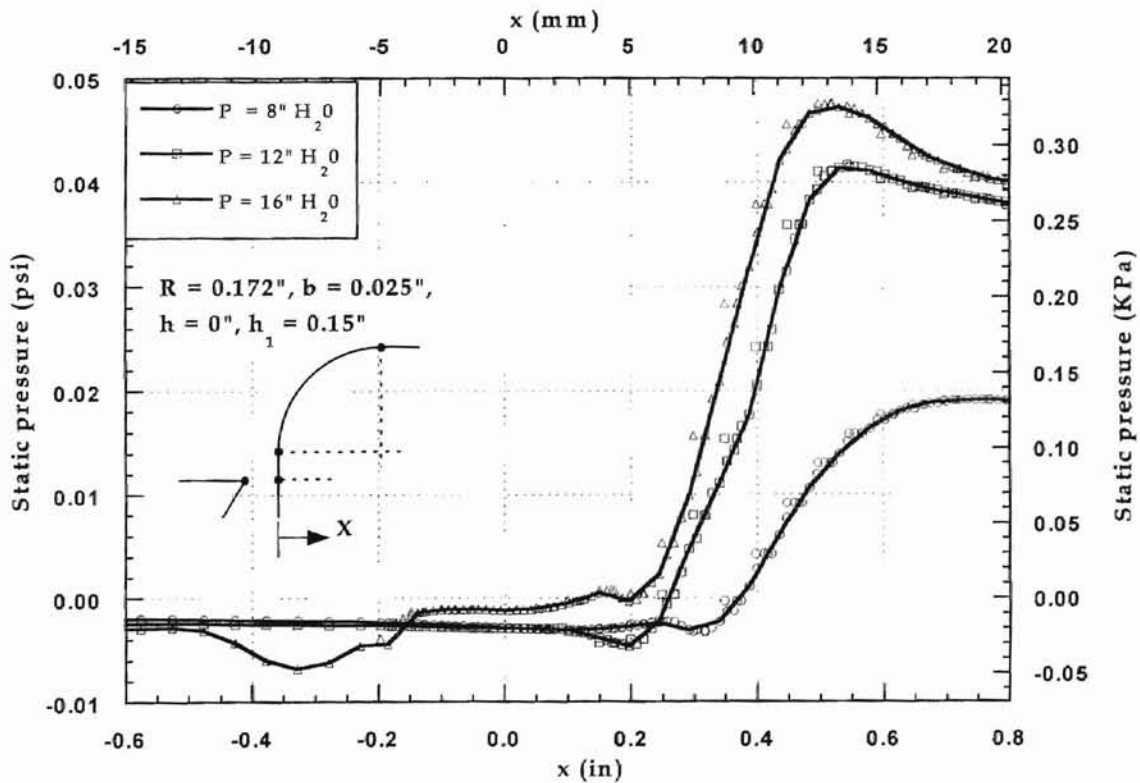
Figure 4.6 Close-up view of pressure distribution on the web for different supply pressures

4.2.2 Aerodynamic friction force on the web

The x-component of the wall shear stress corresponds to the aerodynamic drag on the web. The wall shear stress profile is shown in Fig. 4.7, and it can be seen that it correlates well with the predicted pressure profile. In the region -0.5" < x < 0.5", we find that the shear stress distribution is very oscillatory. The entrained air creates a recirculation due to which we can expect a widely varying shear stress in that region. It is seen that the oscillations shift to the negative x region (x < 0") as the supply pressure is increased .
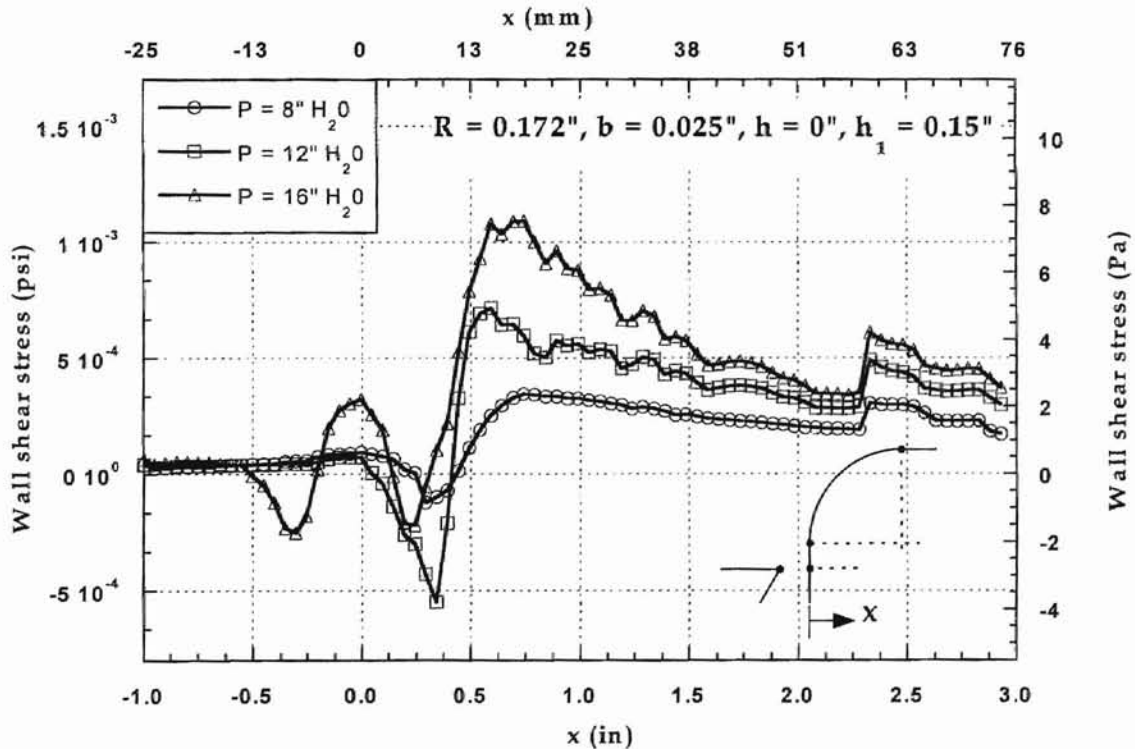
Figure 4.7 Distribution of wall shear stress along the stationary rigid web

A close-up view of the nozzle region wall shear distribution is shown in Fig. 4.8. This figure reveals the shift of the negative peaks in the downstream direction with the increase in supply pressure.
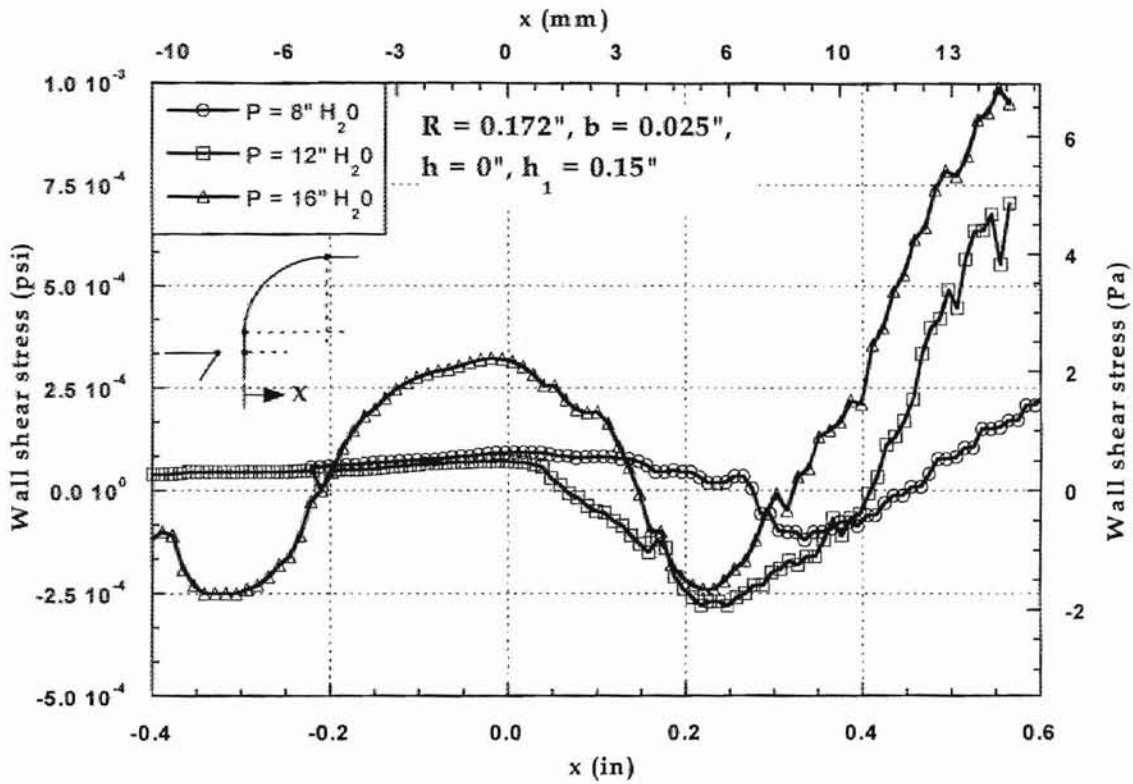
Figure 4.8 Close-up of the wall shear stress profiles for different supply pressures

Figures 4.9, 4.10, and 4.11 show the flow pattern in the nozzle region for different supply pressures. Note the recirculations in the flow created due to the interaction between the entrained air and the mainstream.

Velocity Vectors Colored By Velocity Magnitude (m/s)

Fluent/UNS 4.2 (2d, rsm)
Fri Apr 17 1998
Fluent Inc.
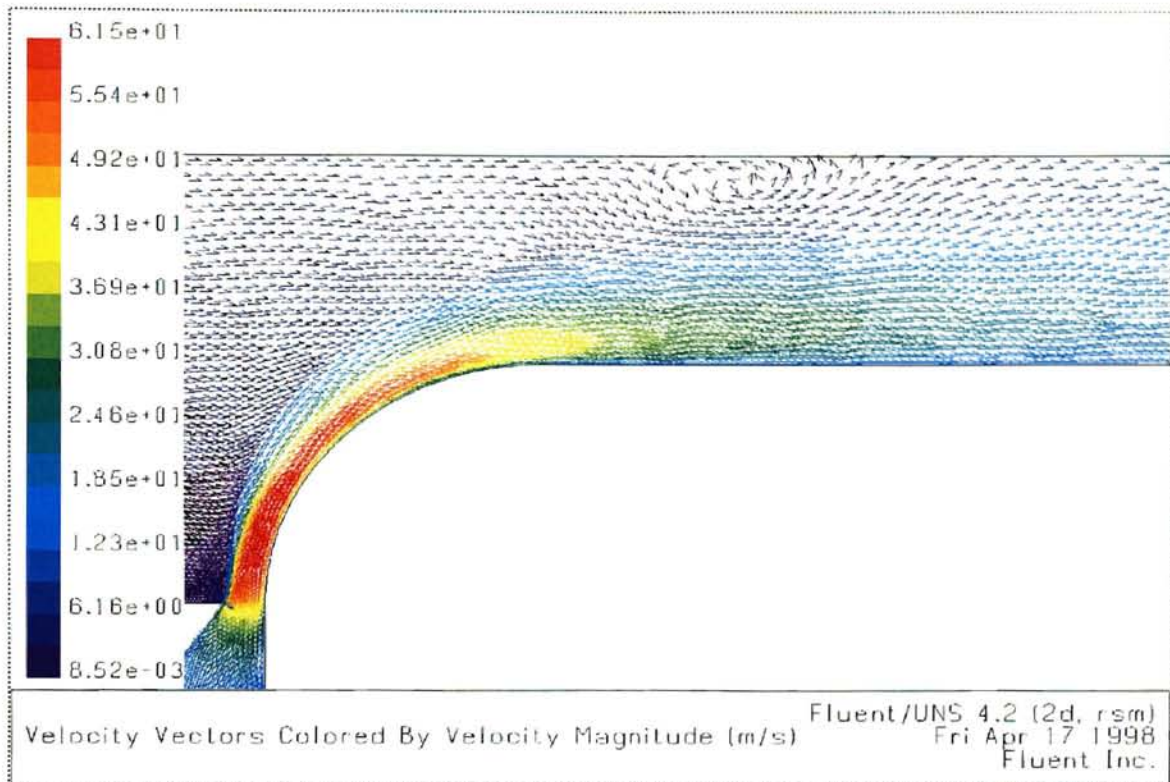
Figure 4.9 Velocity vectors showing recirculation near the nozzle
(P = 8″ H$_2$O, R = 0.172″, b = 0.025″, h = 0″, h$_1$ = 0.15″)

Velocity Vectors Colored By Velocity Magnitude (m/s)

Fluent/UNS 4.2 (2d, rsm)
Fri Apr 17 1998
Fluent Inc.
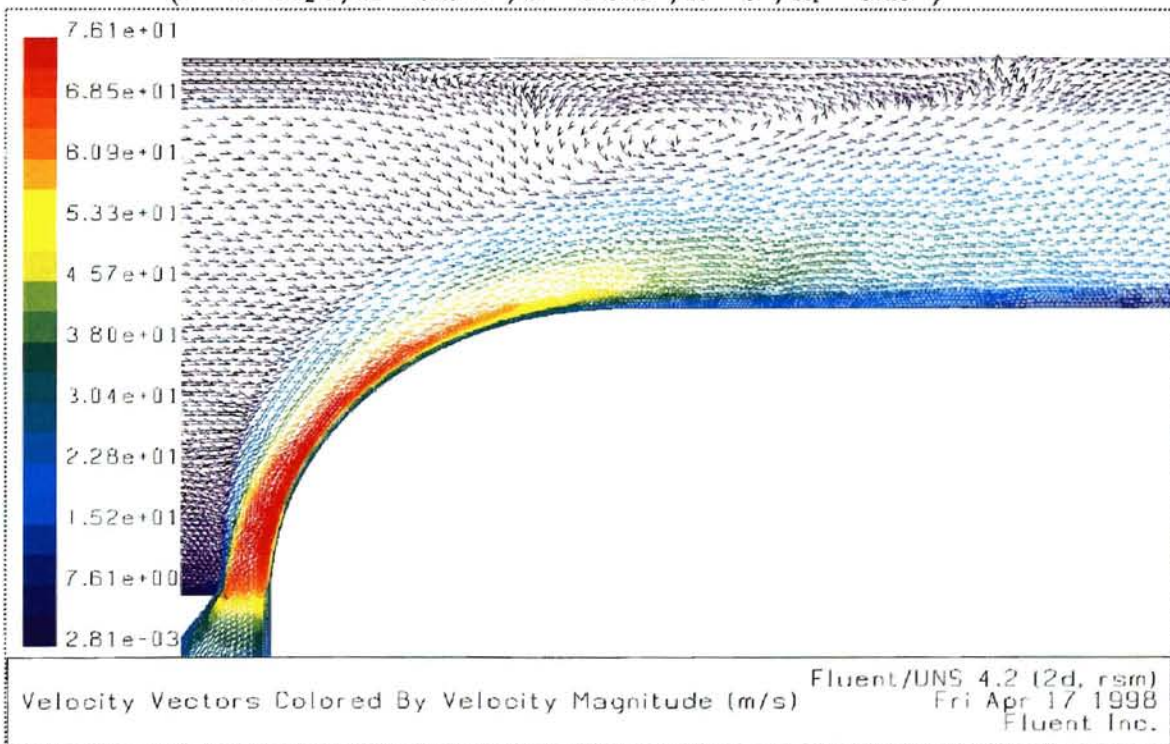
Figure 4.10 Velocity vectors showing recirculation near the nozzle
(P = 12″ H$_2$O, R = 0.172″, b = 0.025″, h = 0″, h$_1$ = 0.15″)
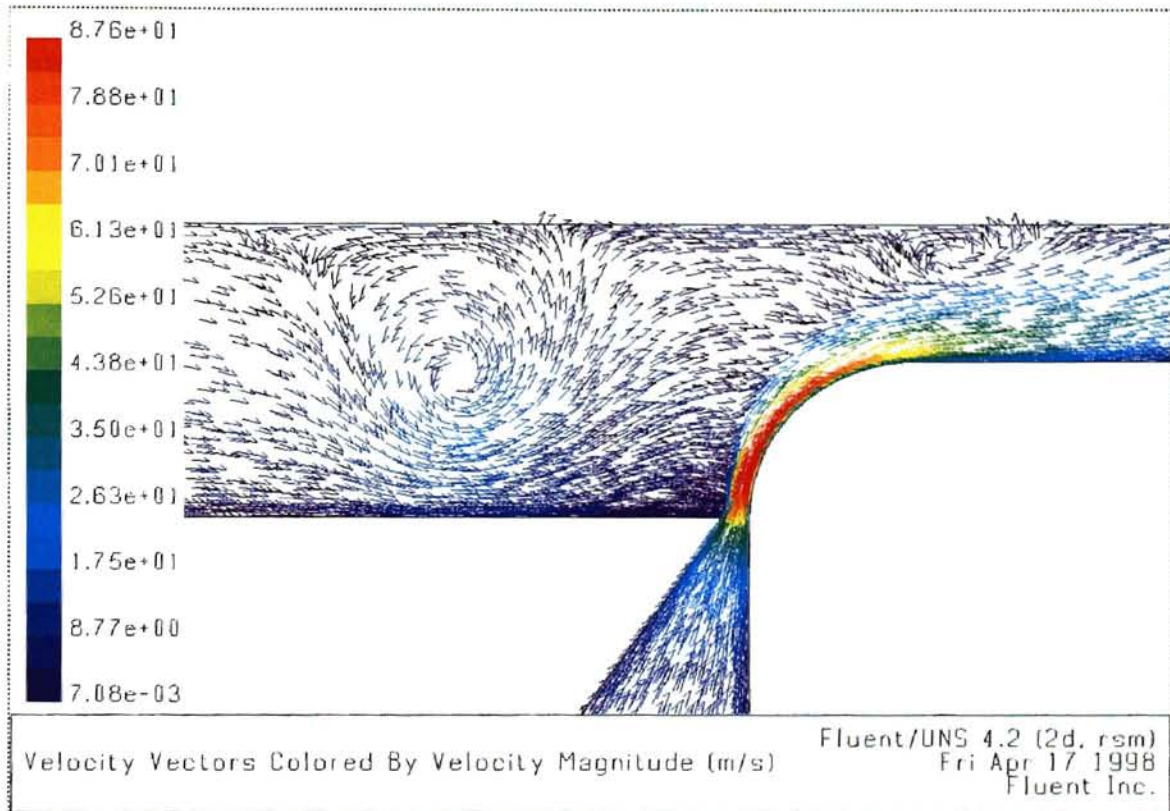
Figure 4.11 Velocity vectors showing recirculation near the nozzle (P = 16″ H_2O, R = 0.172″, b = 0.025″, h = 0″, h_1 = 0.15″)

The most interesting phenomenon that occurs when the air jet interacts with the web is the development of aerodynamic friction force along the web. This force is a direct measure of the capability of the particular configuration to provide sufficient traction to the web. Hence we will study the flow very close to the web, which is where traction is imparted to the web. Figures 4.12 - 4.17 show the comparisons between the velocity vectors close to the web and the corresponding wall shear stress distributions for various supply pressures.

Figures 4.12 and 4.13 are obtained for a supply pressure of 8 in of water. We observe that the recirculation pattern is clearly depicted by the wall shear stress distribution. We can see that the recirculation begins at A_1, and from the slopes of the shear stress between A_1A_2 and A_2A_3 (Fig. 4.12) it seems that the recirculation is composed primarily of the entrained air. We see that at A_2, the local shear stress is a negative peak which means that the traction force is acting against the direction of the web, which is undesirable. We also see that the shear stress gradually becomes zero and eventually becomes positive at A_3. It might be noted that the increase in the shear stress beyond the recirculation zone is rapid, due to the impingement of the air jet on the web. This is clear from Fig. 4.13.

Similar phenomena may be observed from Figs. 4.14 and 4.15, which are obtained using a supply pressure of 12 in. of water. We find that the recirculating zone occurs closer to the nozzle. In other words the increase in supply pressure has shifted the recirculating pattern towards the nozzle ($x = 0$"). Also it may be noted that the recirculating region is more distributed, and the magnitude of the peak negative shear stress (at B_2) is more than twice that at A_2 in Fig. 4.12.

The most interesting phenomenon occurs when the supply pressure is 16 in of water. We have swirl flow both before and after the nozzle. As explained earlier, this might be due to the fact that the jet is subject to rapid

diffusion at higher supply pressures (and hence larger jet widths) and the entrained air gets prevented from entering the floatation region at C_3. This cause a swirl motion before the nozzle region ($-0.4'' < x < -0.2''$) between C_1 and C_3, with the peak negative stress occurring at C_2. However some amount of air can be seen to leave the recirculation and enter the floatation region. This gives rise to another swirl region just after the nozzle ($0.1'' < x < 0.4''$) between C_5 and C_7. From the shear stress profile (Fig. 4.16), it is clear that the peak negative stresses in both the recirculations have the same magnitude of about 2 Pa. This indicates that the swirl component of the recirculating flow is comparable to the main stream flow component.
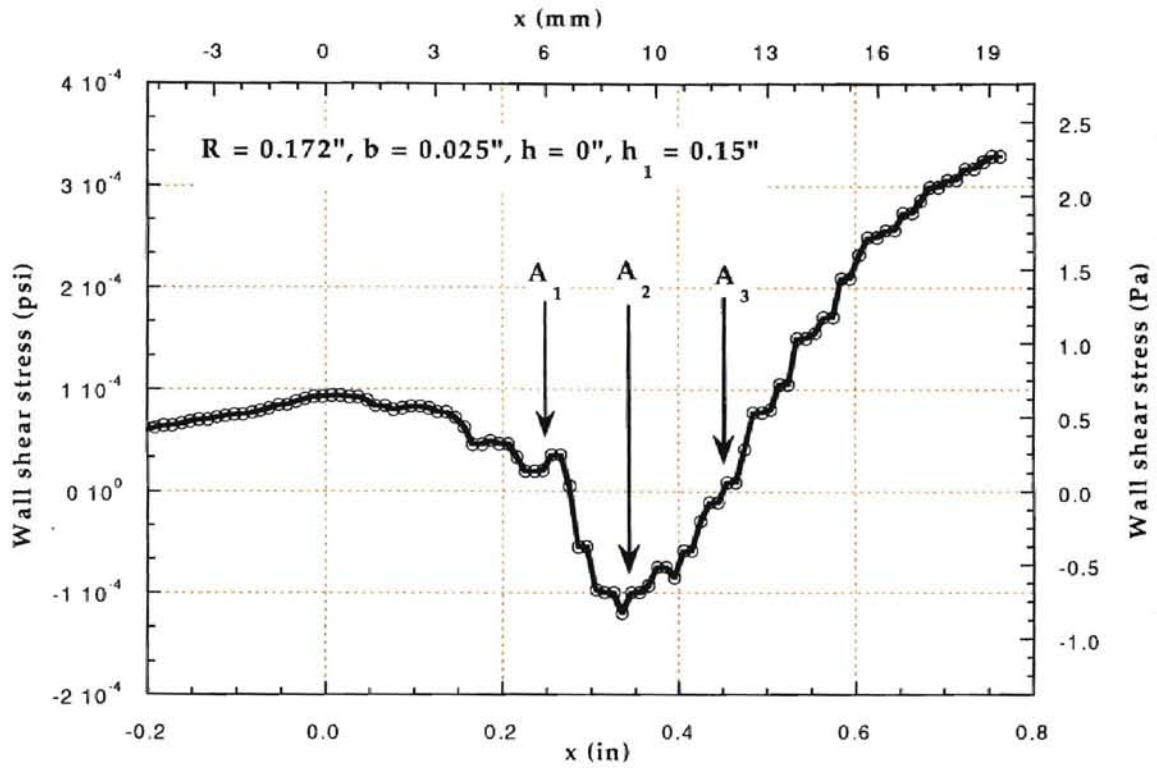
Figure 4.12 Close-up view of the wall shear stress distribution (P = 8" H₂O)

Velocity Vectors Colored By Velocity Magnitude (m/s)

Fluent/UNS 4.2 (2d, rsm)
Fri Apr 17 1998
Fluent Inc.
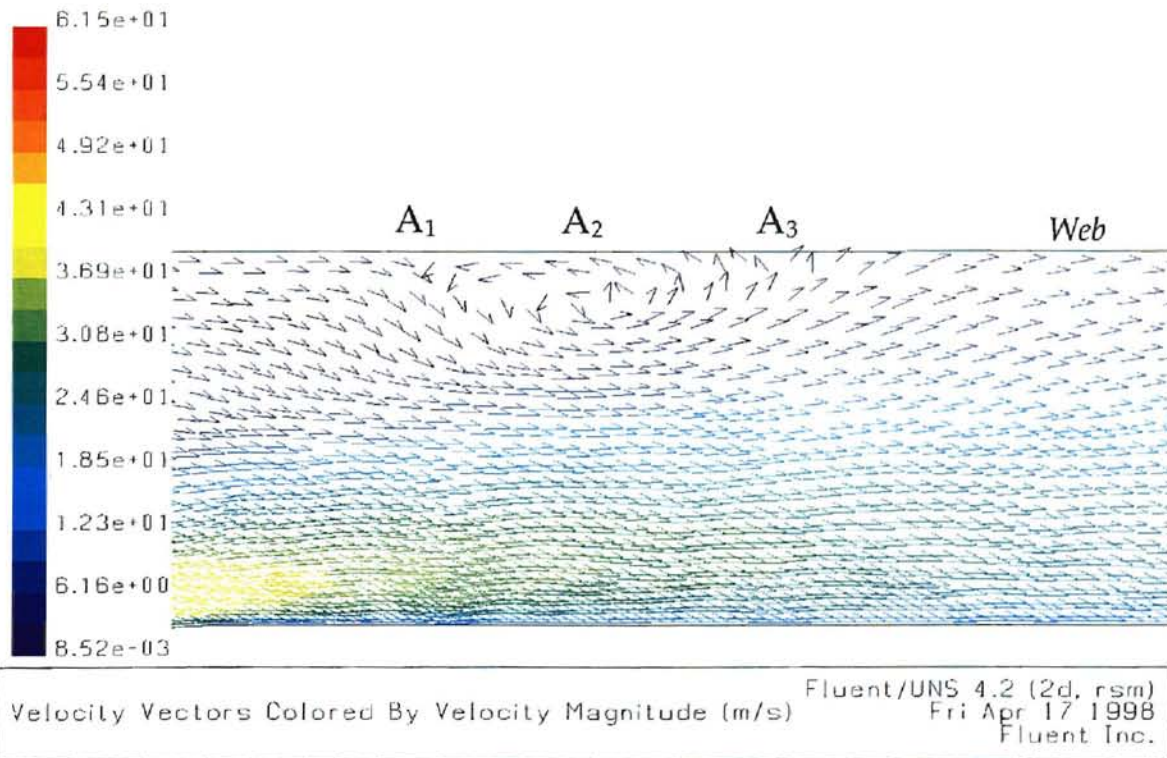
Figure 4.13 Velocity vectors near the web (P = 8" H₂O, R = 0.172", b = 0.025", h = 0", h₁ = 0.15")
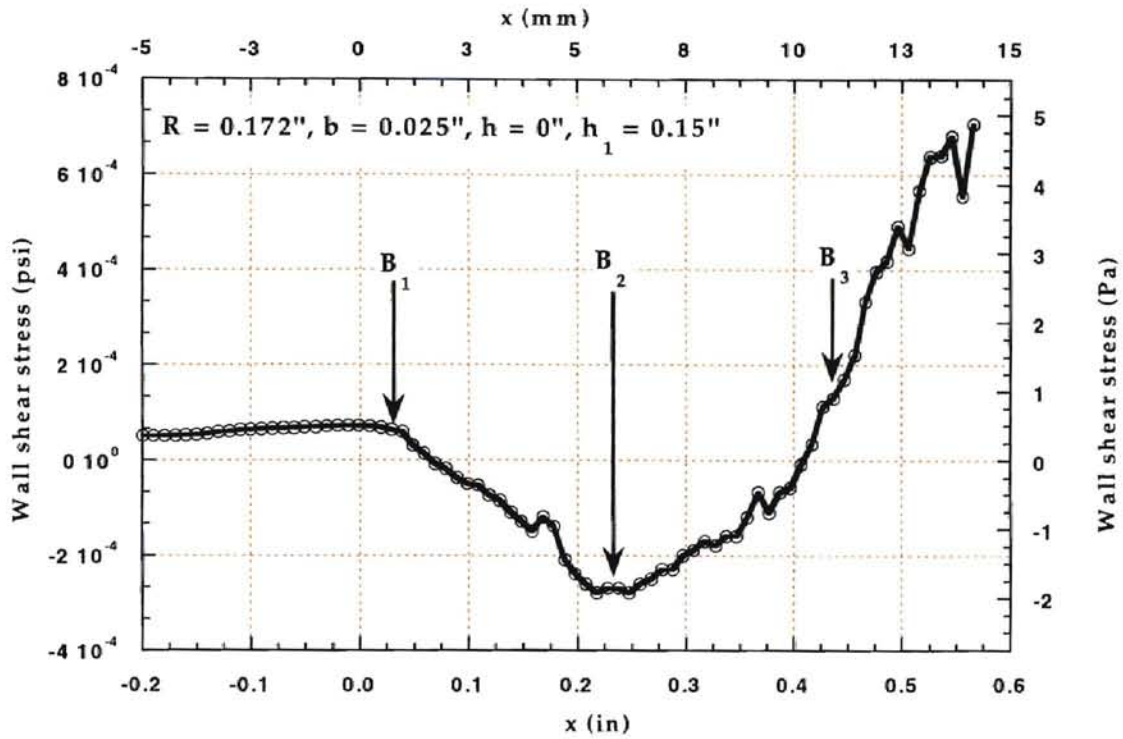
Figure 4.14 Close-up view of the wall shear stress distribution (P = 12″ H₂O)

Velocity Vectors Colored By Velocity Magnitude (m/s)

Fluent/UNS 4.2 (2d, rsm)
Fri Apr 17 1998
Fluent Inc.
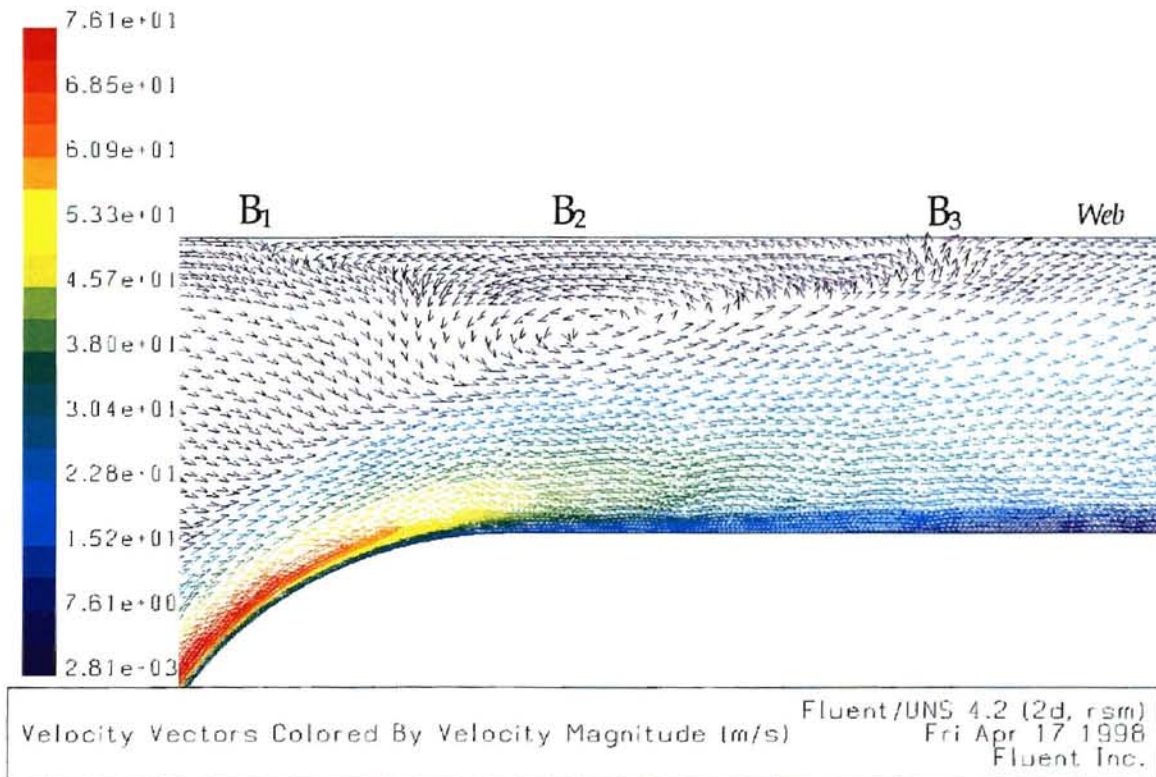
Figure 4.15 Velocity vectors near the web (P = 12 ″ H₂O, R = 0.172″,
b = 0.025″, h = 0″, h₁ = 0.15″)
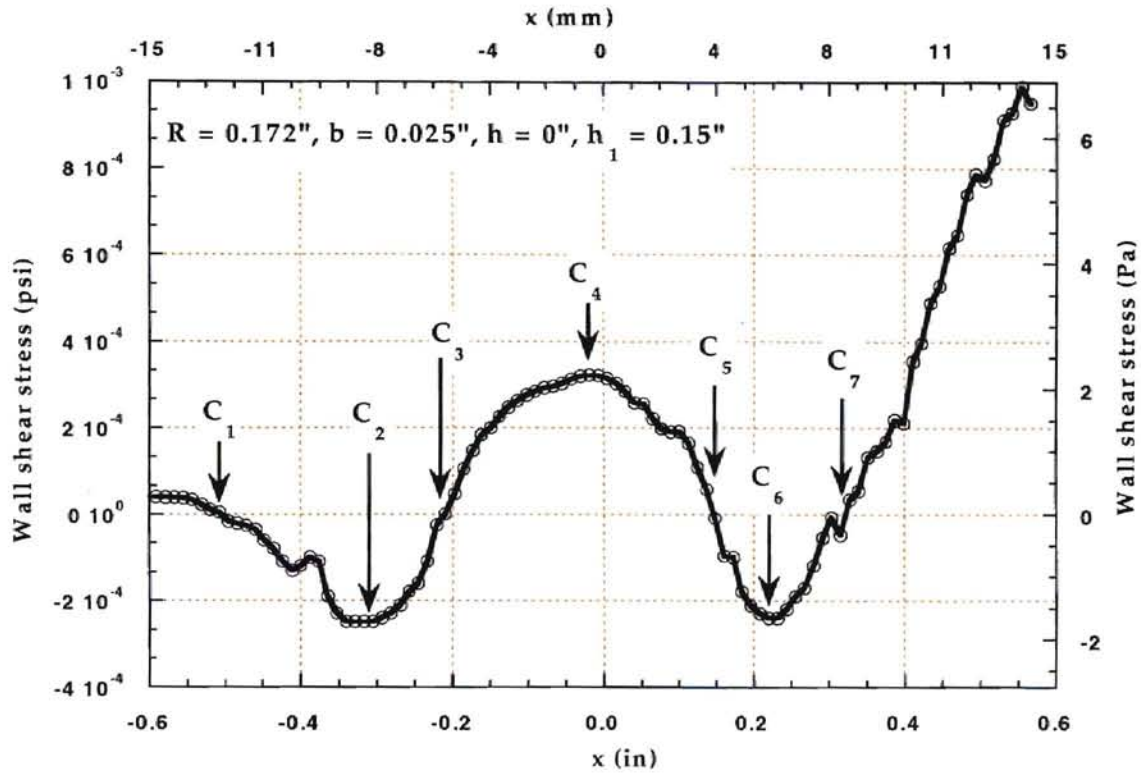
Figure 4.16 Close-up view of the wall shear stress distribution (P = 16″ H₂O)
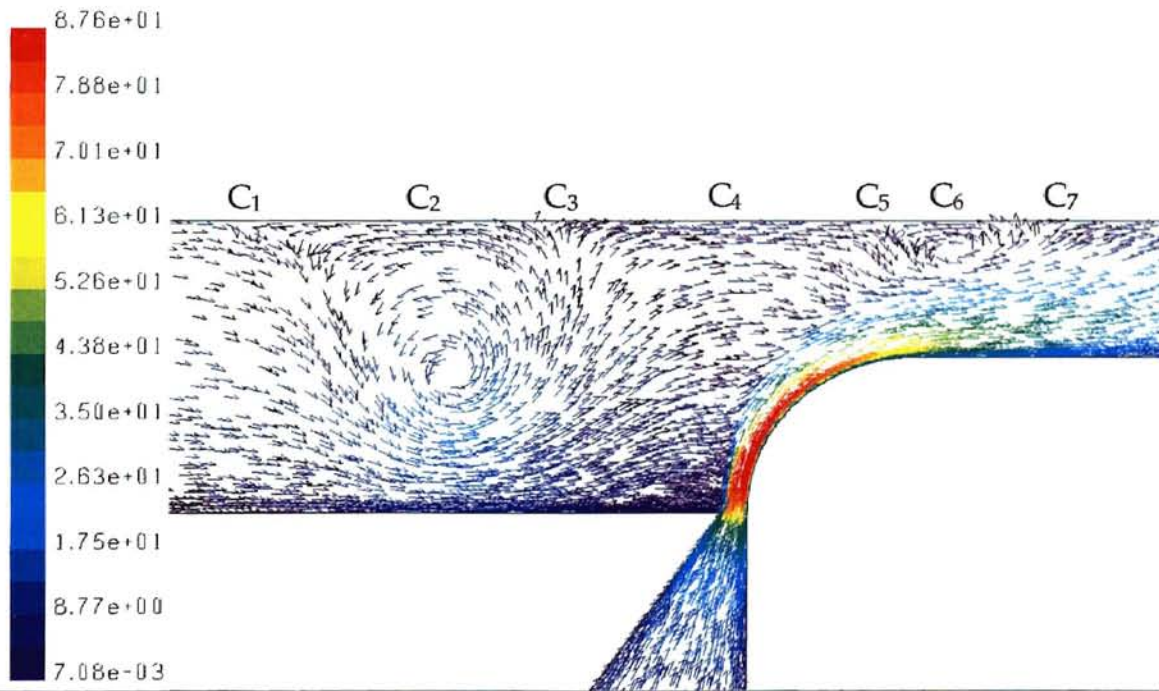
Velocity Vectors Colored By Velocity Magnitude (m/s)

Fluent/UNS 4.2 (2d, rsm)
Sat Apr 18 1998
Fluent Inc.

Figure 4.17 Velocity vectors near the web (P = 16″ H₂O, R = 0.172″, b = 0.025″, h = 0″, h₁ = 0.15″)

It was desired to compare the aerodynamic friction force acting on the web. Integrating the wall shear stress over the entire web gives the average load acting on the web per unit width. Simpson's one-third rule was used to perform the numerical integration over the length of the web. The results obtained from the numerical integration have been presented in Table 4.1 below.

Table 4.1 Integrated aerodynamic friction force on the web for different supply pressures

Supply pressure		Average force on the web per unit width	
inches of water	*KPa*	*lbf/in*	*N/m*
8	1.987	0.0022	0.38
12	2.981	0.0038	0.66
16	3.974	0.0053	0.93

From Table 4.1, we can see that the force acting on the web increases in a constant fashion. This might be due to the fact that the web has been considered as a zero-roughness surface. If the web were to have some roughness imparted to it, then with the increase in the supply pressure, we might expect the force on the web to increase rapidly as the frictional forces come into play.

CHAPTER 5
COMPARISON OF CURRENT STUDY WITH OTHERS

The following is a discussion of the observations made during the computational study of the Coanda effect and it's interaction with a rigid web. The significance of the results obtained are discussed in this chapter. The computational and the experimental observations have been compared to validate the results obtained.

5.1 Coanda Air Jet in Free Space

5.1.1 Effect of supply pressure

When we consider the effect of supply pressure, computational results show that increasing the supply pressure tends to increase the adherence of the jet to the curved surface. Another important observation during the computations was that this behavior of the jet is always true i.e., the jet always gets increasingly adherent to the wall with an increasing supply pressure, irrespective of the values of the other parameters, i.e., the separation critical pressure is always lower than the attachment critical pressure. These results are comparable with Aravamudhan's (1998) experimental results.

5.1.2 Effect of surface roughness

The results obtained by varying the roughness height of the curved surface show that as the roughness height increases, the upper critical pressure

required for the attachment of the jet to the wall decreases. This is in accordance with a previous study (Zhang and Ko, 1996). The results obtained thus confirm that the curved surface close to the jet might be roughened to improve jet attachment.

5.1.3 Effect of nozzle offset

The nozzle offset h was found to have a very prominent effect on the jet behavior. Several results have been obtained by varying the nozzle offset value between 0" and 0.1". It was found that when h = 0", changing the nozzle width b from 0 " to 0.06" resulted in the upper critical pressure to increase rapidly. Then h was fixed at 0.1" and the nozzle width b was varied between 0" and 0.06". Now we can see that the upper critical pressure is not affected very much by the change in nozzle width. This drastic change occurs for a change in nozzle offset from 0" to 0.1". These results have been verified experimentally by Aravamudhan (1998). A comparison of the experimental and computational result is shown in Fig. 5.1.
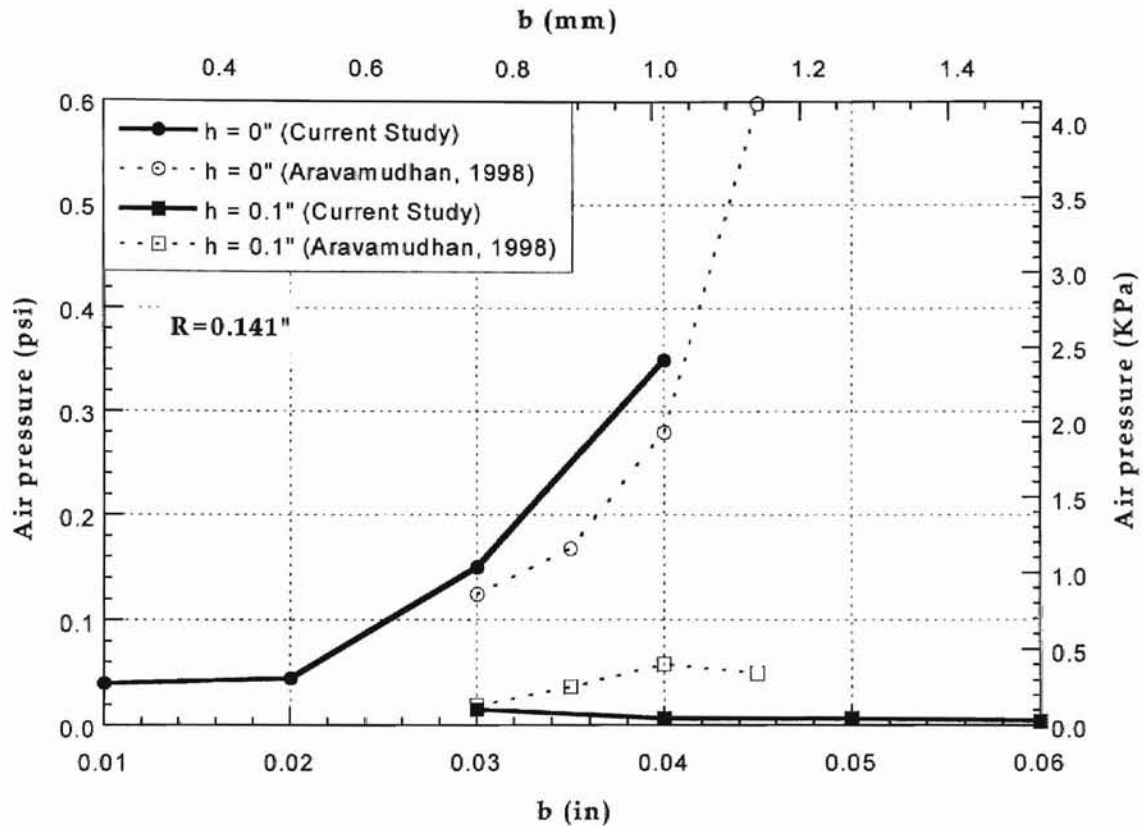
Figure 5.1 Effect of nozzle offset - comparison of computational results with Aravamudhan's experiments (1998)

These results indicate that the increase in h is favorable in that the jet becomes attached even at low supply pressures. But from the study of the interaction between the web and the Coanda air jet, we know that a low pressure will yield a smaller force on the web (see Table 4.1). Hence at such low pressures the traction force required for transporting the web might not be enough.

The reason for the quantitative variations in Fig. 5.1 could be explained as follows. In the experimental study, the method of determining the attachment or separation of the jet was to use the hand to "feel" the direction of flow. But in this computational study, the attachment or separation of the jet was determined by

examining the flow velocity contours and the velocity vector plots. This is obviously a more accurate way of determining the pattern of the air jet. Hence when the two data sets need to be compared, they certainly cannot be expected to match exactly. The fact that they match in a qualitative manner (showing similar trends) means that there does exists a trend or pattern in the change of critical pressure with respect to change in other parameters.

5.2 Interaction with a Stationary Rigid Web

The computed pressure distribution shows similar trends with experimental results obtained by Aravamudhan (1998) as shown in Fig. 5.2. However, the magnitudes of the computed pressures are higher than experimental results.
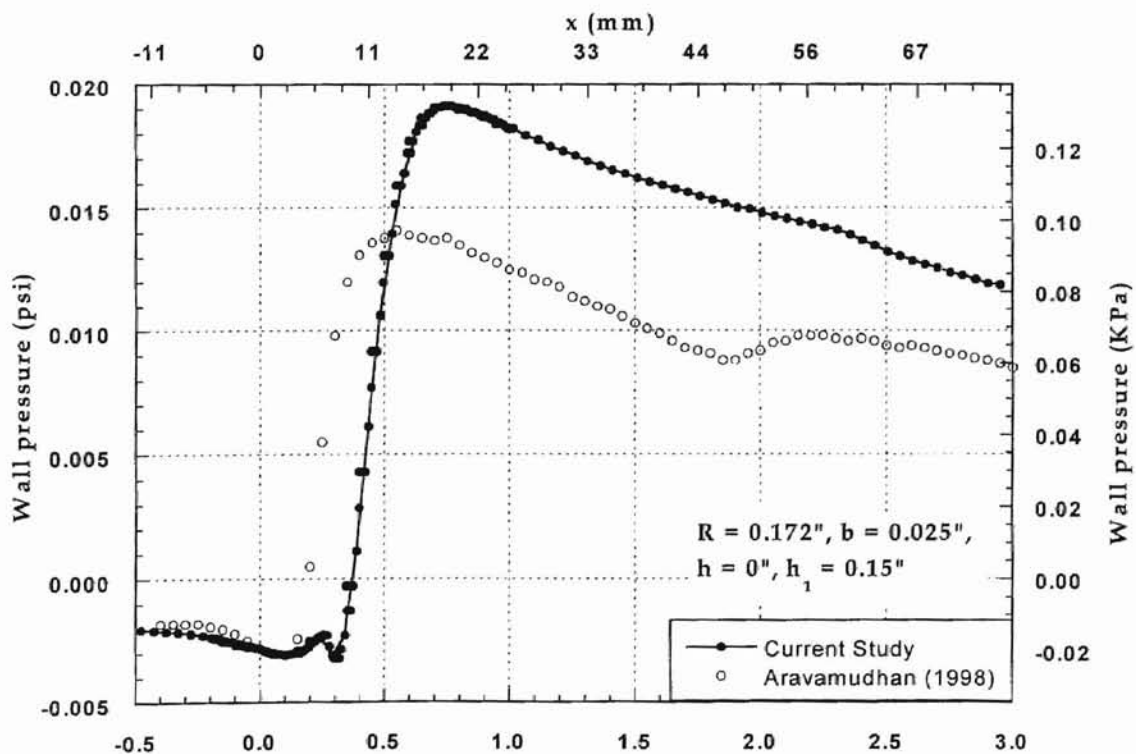
Figure 5.2 Comparison of pressure profiles with Aravamudhan's experiments (1998) (R = 0.141″, b = 0.025″, h = 0″, h_1 = 0.15″, P = 8″ H$_2$O)

This could be attributed to the edge leakage effect in the experimentation, since a finite width web was used. And so there existed a small gap between the web and the side-walls which could not be avoided. But computation of the model was two-dimensional, and the edge leakage was not considered at all. At the same time, though the mesh used for computations was very fine, it may not be fully sufficient to resolve the flow. This could be the reason for the quantitative discrepancy in the results obtained.

If we compare the experimental and computational pressure profiles near the nozzle (Fig. 5.3), we see that the profiles show good agreement with each other, up to x = 0.35". After that, the computational results are found to depart from the experimental results. This might be due to insufficient mesh resolution in that region.
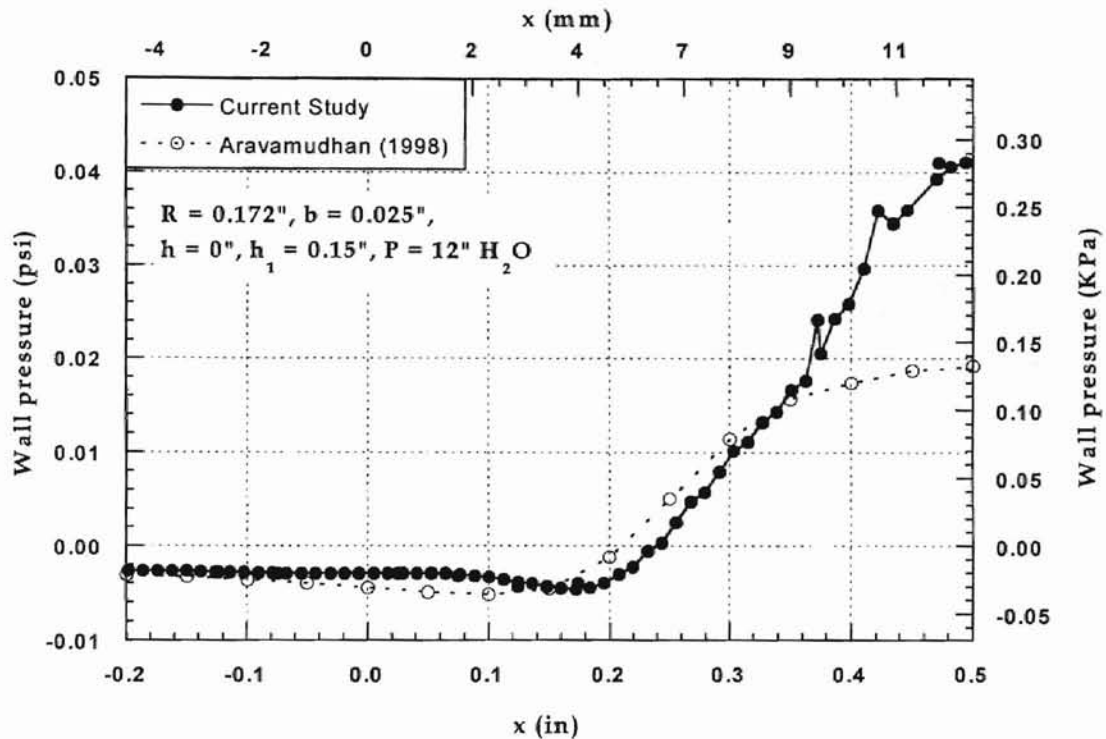
Figure 5.3 Comparison of pressure distribution near the nozzle (P = 12″ H₂O)

If the mesh size was increased, this automatically increases the cell-linkage data (of the mesh), in an exponential manner, thus slowing down the calculation process drastically. As is, the calculations for the stationary rigid web took more than 36 hours for convergence on a multi-processor workstation. Any more optimization of the mesh would certainly make the calculation impractical.
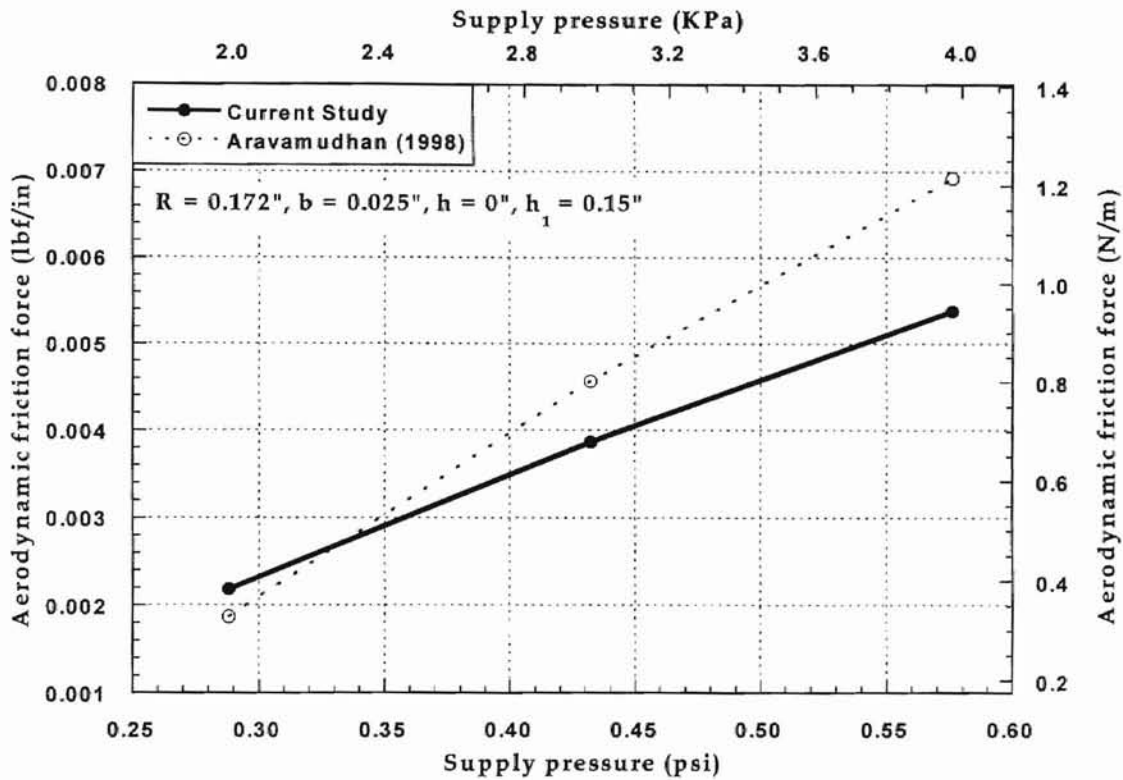
Figure 5.4 Comparison of computed force on the web with Aravamudhan's
experiments (1998)

As the experimental results yielded only an average value for load,
numerical integration was performed on the computed shear stress to obtain the
average frictional load on the web. The results are compared as shown in Fig. 5.4.

We find a general agreement of the computed aerodynamic frictional
force values at different supply pressures with Aravamudhan's experimental
work (1998). It can also be noted that as the supply pressure is increased from 8
in of water to 16 in of water, the computed force value falls behind the
experimental values. This might be due to the fact that the computational model
considered the web to have a zero surface roughness, whereas in practice the
web does have some roughness. For laminar internal flow, friction loass does not

depend on surface roughness unless the surface is extremely rough. For turbulent flow, however, friction loss increases with surface roughness. Current study model is much different from fully developed internal flow problem. However, the fact that the computed friction forces for smooth web fall below the experimental results for less smooth web seems to be in line with the internal flow analogy.

CHAPTER 6
CONCLUSIONS

From the observations made during this computational research, the following concluding remarks can be made. A few guidelines and suggestions for designing and operating air-floatation devices have also been given.

1. Computational study shows that the Coanda air jet exhibits three distinct regions or flow patterns: attached flow region in which the air jet is always attached to the surface, separated flow region in which the jet always remains separated bistable region. In this bistable region it has been found that the flow can be either attached or separated, depending on the type and direction of the influence. The existence of these three distinct regions means that the operating supply pressure should always be above the upper critical pressure for that configuration for the jet to remain always attached.

2. The increase in roughness of the surface was found to increase the adherence of the jet to the curved surface. This complies with the general observation that the existence of grooves in the surface increases the tendency op adherence (Zhang and Ko, 1996). Hence, when designing air floatation devices, the surface adjacent to the jet can be roughened to enhance attachment.

3. As h increases from 0", the threshold pressure for attachment drops suddenly

at around 0.05″ or 0.1″ (1.27mm or 2.54 mm) and then increases slightly. In the range of values tested, h = 0.1″ is found to be the optimum value. For configurations above and below this value of h, the upper critical pressure is found to be higher. Hence, from the design point of view, it is recommended to use 0.05″ < h < 0.1″ to improve attachment.

4. Another guideline would be to use a smaller value of b, as this was seen to reduce the upper critical pressure. A value of b < 0.03″ can be considered to be a suitable value. Again, this depends on the the nozzle offset h. Calculations show that the value of b matters only when 0.0″ < h < 0.05″. When h > 0.05″, the upper critical pressures seem to be independant of b. These combined effects of h and b can be crucial during the design and operation of air floatation devices.

5. Study of the interaction of the Coanda air jet with a stationary rigid web shows that some air is entrained from the nozzle upstream into the mainstream.

6. Recirculatory patterns can exist in the region where the entrained air mixes with the mainstream. As the supply pressure increases, these recirculations have been found to shift upstream of the nozzle region.

7. Calculation results for different supply pressures reveal that the change in magnitude of the pressure peaks is not proportional to the supply pressure. This means that there exists a upper supply pressure value, beyond which

any increase in the supply pressure might not contribute much to the

pressure exerted on the web.

CHAPTER 7
RECOMMENDATIONS FOR FUTURE STUDY

Based on the computational study conducted on the Coanda air jet, it was found that a variety of improvements could be made to the computational models that would be created in the future. The following discussion is based on the observations made during the course of this research study.

1. For more accurate determination of the upper and lower critical pressures, it is suggested that the behavior of the jet over a wider range of supply pressures be analyzed, by computing several solutions using finer steps of supply pressures.

2. A more rigorous method of establishing the condition of the jet (as attached or separated) from computational results should be formulated.

3. A universal concern with any computational model is the size of the mesh generated and the computing time associated with it. Especially when using Fluent's in-built capability to refine meshes based on gradients of solutions, the user has to be careful to properly balance the amount of accuracy actually required and the corresponding increase in the size of the mesh.

4. One suggestion pertinent to the Coanda air jet model is that, a better representation of the flow outlet boundary might reduce the size of the mesh and hence cut down computing time. The use of a PRESSURE-OUTFLOW BC at

the outlet boundary which models atmospheric conditions, requires it to be placed at a considerable distance from the nozzle to avoid the numerical constraint on the jet, which would occur otherwise. Unfortunately this has the undesirable effect of increasing the size of the mesh without contributing much to the actual region of interest i.e., nozzle region.

5. The computations for interaction between the air jet and the stationary rigid web could be extended to investigate the effect of floatation height, nozzle width, nozzle offset, etc.

6. The effect of different types of adjacent surfaces could be studied. It has been claimed (Reba, 1966) that the existence of a small step in the curved region, results in better adherence tendency of the jet. A computational study could be done to establish this quantitatively.

7. A 3D model could be built and used for the computations. Though this would admittedly increase the calculation time, it certainly would give us more insight into the physics of the flow. Currently, with a 2D model, variation of parameters (pressure, force, etc.,) only in the machine direction of the web can be studied. A 3D model enables us to study the cross flow also.

8. The current study assumes that the stationary rigid web is perfectly smooth. Future work could involve webs with a variety of surface roughness. Increased friction on the web surface might introduce interesting changes in

the pressure distribution.

9. The interaction between the Coanda air jet and a stationary rigid web has been studied. This model can be extended to accommodate a flexible moving web.

REFERENCES

Aravamudhan, V., "An Experimental Study of the Behavior of the Coanda Jet and Its Application to Web Support and Traction," *MS Thesis*, Oklahoma State University, 1998.

Bourque, C. and Newman, B. G., "Reattachment of a Two-Dimensional Incompressible Jet to an Adjacent Flat Plate," *The Aeronautical Quarterly*, Vol. XI, August 1960.

Boussinesq, J., "Theorie de l'ecoulement tourbillant," *Mem. Pre. par. div. Sav. 23*, Paris, 1877.

Bradshaw, P., Ferriss, D. H. and Atwell, N. P., "Calculation of Boundary Layer Development Using the Turbulent Energy Equation," *Journal of Fluid Mechanics*, vol. 28, p. 593, 1967.

Brown, G. L. and A. Roshko, "On Density Effects and Large Structure in Turbulent Mixing Layers," *Journal of Fluid Mechanics*, vol. 64, pt. 4, pp. 775-816, 1974.

Davidson, L., "Reynolds Stress Transport Modeling of Shock-Induced Separated Flow," *Computers and Fluids*, Vol. 24, No. 3, pp. 253-268, 1995.

Felsing, G. W. and Moller, P. S., "Coanda Flow Over a Circular Cylinder With Injection Normal to the Surface," *AIAA Journal*, Vol. 7, No. 5, pp. 842-846, 1969.

Gheorghiu, C., "Romanian Inventions and Priorities in Aviation," Ed. Albatros, Bucharest, 1979 (in Romanian).

Gregory-Smith, D. G. and Gilchrist, A. R., "The Compressible Coanda Wall-jet : An Experimental Study of Jet Structure and Breakaway," *International Journal of Heat and Fluid Flow*, Vol. 8, No. 2, June 1987.

Jorgenson, C. E. and Pletcher, H., "An Implicit Numerical Scheme for the Simulation of Internal Viscous Flow on Unstructured Grids," *Computers and Fluids*, Vol. 25, No. 5, pp. 447-466, 1996.

Kolmogrov, A. N., "Equations of Turbulent Motion of an Incompressible Turbulent Fluid," *Izv. Akad. Nauk SSSR Ser Phys. VI*, No. 1-2, p. 56, 1942.

Launder, B. E. and Spalding, D. B., *Lectures in Mathematical Models of Turbulence*, Academic, New York, 1972.

Lilek Z. and Peric M., "A Fourth-Order Finite Volume Method with Colocated Variable Arrangement," *Computers and Fluids*,Vol. 24, No. 3, pp. 239-252, 1995.

Morrison, J. F. and Gregory-Smith, D. G., "Calculation of an Axisymmetric Turbulent Wall Jet over a Surface of Convex Curvature," *International Journal of Heat and Fluid Flow*, Vol. 5, No. 3, September 1984.

Murai, K., Kawashima, Y., Nakanishi, S., and Taga, M., "Self-Oscillation Phenomena of Turbulent Jets in a Channel," *Canadian Journal of Chemical Engineering*, Vol. 67, pp. 906-911, 1989.

Prandtl, L., "Bericht uber Untersuchungen zur ausgebildeten Turbulenz," *ZAMM*, vol.5, p. 136, 1925.

Reba, I., "Applications of the Coanda Effect," *Scientific American*, Vol. 214, No. 6, pp. 84-92, 1966.

Richmond, M. C., "Convex and Concave Surface Curvature Effects in Wall-Bounded Turbulent Flows," *AIAA Journal*, Vol. 29, No. 6, June 1991.

Rodman, L. C., Wood, N. J., and Roberts, L., "Experimental Investigation of Straight and Curved Annular Wall Jets," *AIAA Journal*, Vol. 27, No. 8, August 1989.

Sharif, M. A. R. and Wong, Y. K. E., "Evaluation of the Performance of Three Turbulence Closure Models in the Prediction of Confined Swirling Flows," *Computers and Fluids*, Vol. 25, No. 5, pp. 332-345, 1996.

Squire, H. B., "Jet Flow and It's Effect on Aircraft," *Aircraft Engineering*, Vol. 22, March 1950.

Tattersall, P. and McGuirk, J., "Evaluation of Numerical Diffusion Effects in Viscous Flow Calculations," *Computers and Fluids*, Vol. 23, No. 1, pp. 177-209, 1994.

Yoshihiro I., "A Study on the Deflection and Reattachment of an Axisymmetric Radial Wall Jet (Deflection of Main Jet near Nozzle)," *JSME International Journal*, Vol. 30, No. 266, 1987.

Von Karman, T. H., "Mechanische Ahnlichkeit und Turbulenz," *Proceedings of 3rd International Congress on Applied Mechanics*, Stockholm, pt. 1, p. 85, 1930.

Zhang, H. L. and Ko, N. W. M., "Numerical Analysis of Incompressible Flow Over Smooth and Grooved Circular Cylinders," *Computers and Fluids*, Vol. 25, No. 3, pp. 261-281, 1996.

APPENDIX
PROCEDURE OF USING FLUENT TO ANALYZE THE COANDA AIR JET

This chapter will explain in detail the steps involved in using FLUENT/UNS (UNS stands for "UNStructured") to analyze the Coanda jet. It should be understood that only the key steps in creating and solving this specific model are presented here. For more elaborate explanations, the reader is advised to refer the FLUENT/UNS vols.1-4.

The following are the steps involved in solving any problem using FLUENT/UNS.

- Definition of the Modeling Goals

    What specific results are required from the model?

    What degree of accuracy is required from the model?

- Choice of Computational model

    Where will the model domain begin and end?

    What boundary conditions will be used ?

    Will a 2D grid be sufficient to accurately describe the geometry, or will a 3D model be necessary?

- Choice of Physical models

    Is the flow laminar or turbulent?

    Is the flow going to compressible or incompressible?

- Determination of the solution procedure

    Will changing some default parameters accelerate convergence?

    The actual problem solving steps are as follows.

Step 1 :   Create the model geometry and grid.

Step 2 :   Start the appropriate solver for 2D or 3D

Step 3 :   Import the grid

Step 4 :   Check and scale the grid, if necessary.

Step 5 :   Choose the models and equations to be used in the solving process.

Step 6 :   Specify material properties.

Step 7 :   Specify the boundary conditions.

Step 8 :   Adjust solution control parameters.

Step 9 :   Initialize the flow field.

Step 10 :   Calculate the solution.

Step 11 :   Examine the results.

Step 12 :   If necessary, refine the grid and continue the solution process.

Step 1 : Create the model geometry and grid

This first and foremost step of the solution process requires a geometry modeler and a grid generator. Any popular modeling program may be used for modeling the geometry, because of FLUENT's capability to import a variety of file formats. For the simplest models, FLUENT has in-built modeling and meshing capabilities. In almost all other cases, GeoMesh, which comes along with FLUENT will have to be used. As we have a rather complex geometry, we will use GeoMesh for our modeling purposes. GeoMesh may be started by typing :

$ geomesh

at the command prompt. The flow of information between GeoMesh and FLUENT may be depicted as follows.
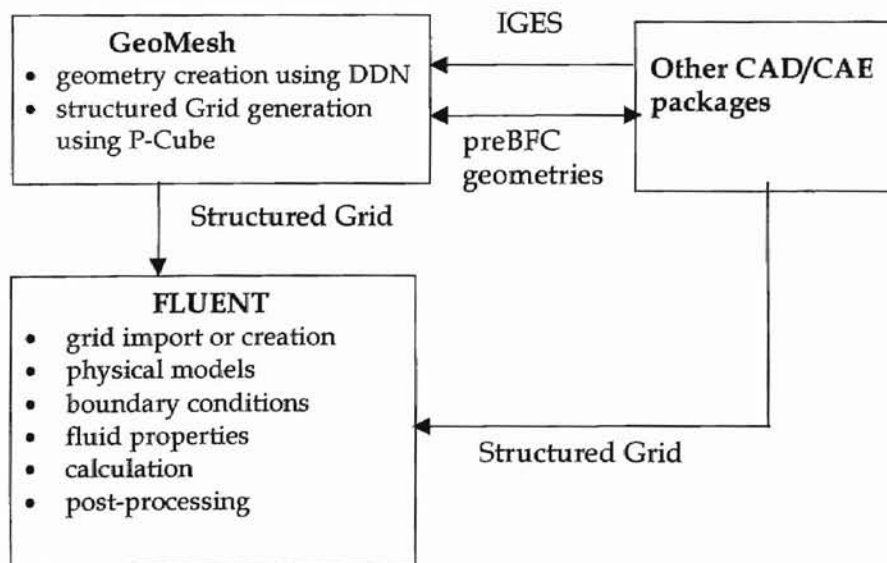
Figure A.1 Information flow between various packages

The user is required to create a new configuration. The configuration is a sub-directory in which a copy of the geometry and all meshing related files will be stored. This may be done by using the NEW CONFIGURATION option from the CONFIGURATION menu. Now, selecting DDN from the APPLICATIONS menu starts the DDN program. The geometry we have chosen to model is given in Fig. A.2 .
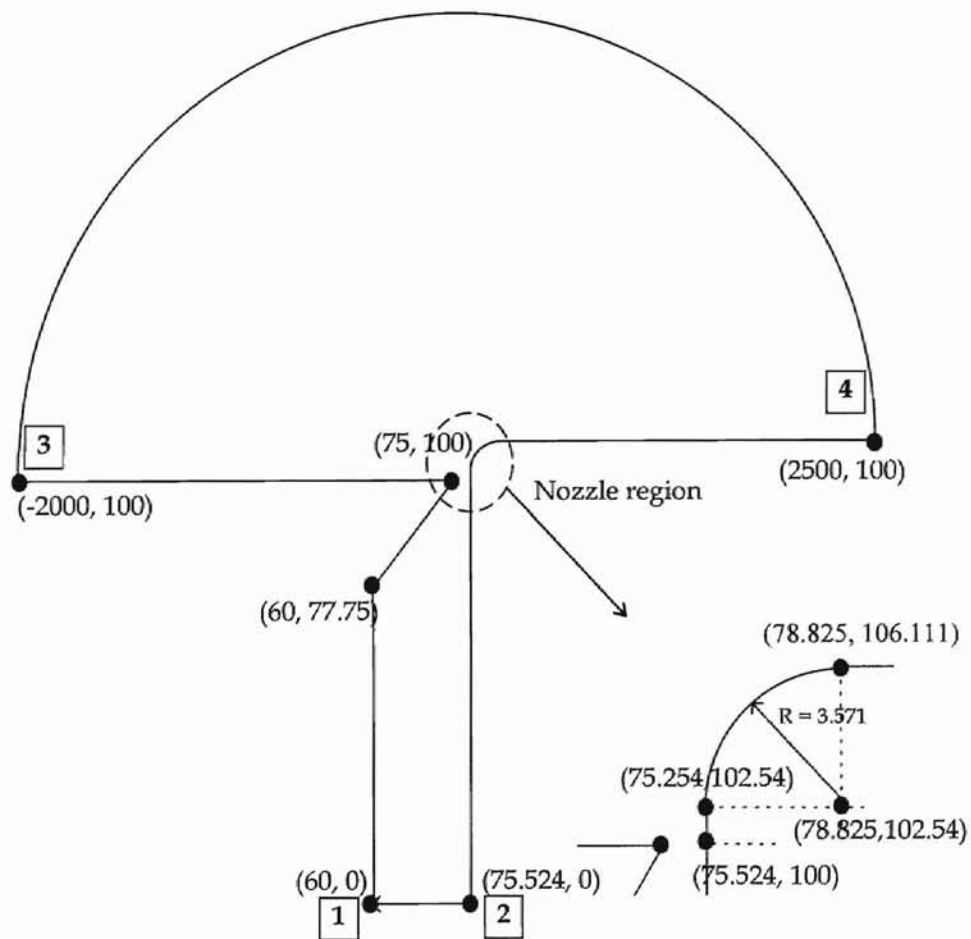
Figure A.2 Dimensions of the Coanda air jet model (in mm)

In DDN, we will draw only the points and curves of the geometry (shown above) which will guide us in creating the grid in P-Cube. Before attempting to draw, the user needs to be familiar with the mouse button functions. (Please refer to Chapter 3, GeoMesh manual.) Once we are inside DDN, we may draw the points by clicking on the POINT option and following the instructions. At any point, we may press F9 to zoom and pan the drawing. After all the points have been created, the curves may be drawn using the ARC/CIRCLE/FILLET option in the main menu. At this point, the geometry looks like shown below. We may now save and exit by choosing FILE/QUIT.

In the GeoMesh window, the above geometry part is chosen (by clicking on it) and then copied to the meshing-parts window. We may now start P-Cube, which will be used to create the grid describing the geometry, by double-clicking on the part name in the meshing-parts window.

The first thing that needs to be input to P-Cube is the type of grid that is needed to be generated. This information can be input through the Startup Modals dialog box shown in Fig. A.3. Click on 3D-HEX and change it to 2D-TRI, which the type of grid that we need. Also change the analysis code to Fluent/UNS. All other information may be left unchanged.
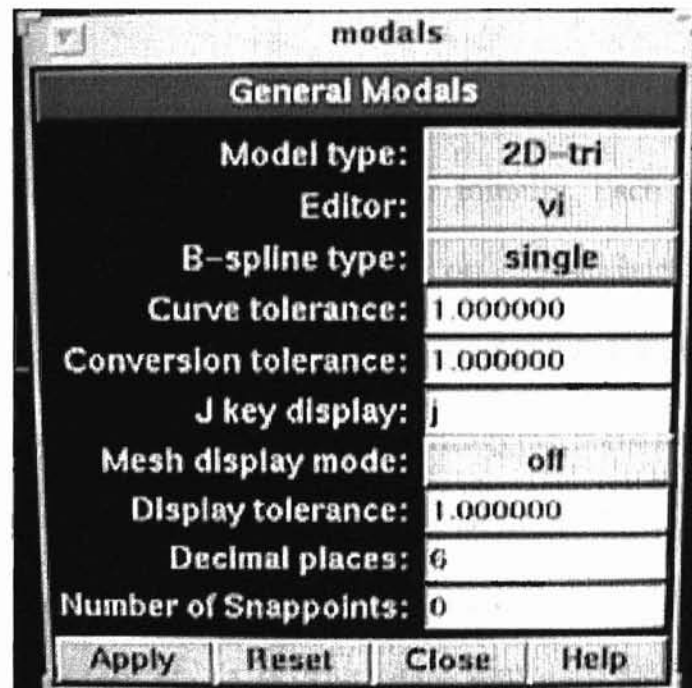
Figure A.3 Startup-Modals Box

At this point all the points and curves that we created using DDN should appear on the screen. If they don't, press the MAX button on the bottom of the screen to show the entire geometry on the screen. Our objective now is to create edges along the points and curves we have drawn, to enclose the model, or in other words, to create the "solution domain". The edges will then be assigned appropriate boundary conditions.

P-Cube has a "domain topology" concept, which should be thoroughly understood. The "domain topology" consists of edges and/or faces and describes how they are connected to each other. This domain topology is then overlaid on the geometry. One of the important attributes is that adjacent faces should share common edges (in 2D) and adjacent blocks should share common

faces (in 3D).

We will now create a face to encompass the entire solution domain. Each face by default has 4 edges and is rectangular initially. Each edge might be broken into any number of sub-edges later. Click on CREATE button and then on the FACE button. We now have a face. The corners of the face might be attached to vertices, by double-clicking on them and then dragging them to the right place (The "intersection -snap" mode may be used to exactly fix the corners in place). Each numbered corner of the face is fixed to the correspondingly numbered vertex of the geometry (see Fig. A.4). The edges will now be "bent" at a few places to conform to the shape of the geometry.

Choose the 1-3 edge of the new face, and then right-click on the edge. This will "break" the edge into two at that point. This vertex is attached to the appropriate point of the geometry, as indicated by the arrowline in the figure.

Now the face has 5 edges. Similarly, the other edges might be "broken" into as many edges as required to conform to the boundary of the geometry. Note that the edge 3-4 needs to be conformed to the top curve, and it can be done in a similar way, except keeping the CURVE button on, rather than the EDGE button and using the "d-snap" mode.
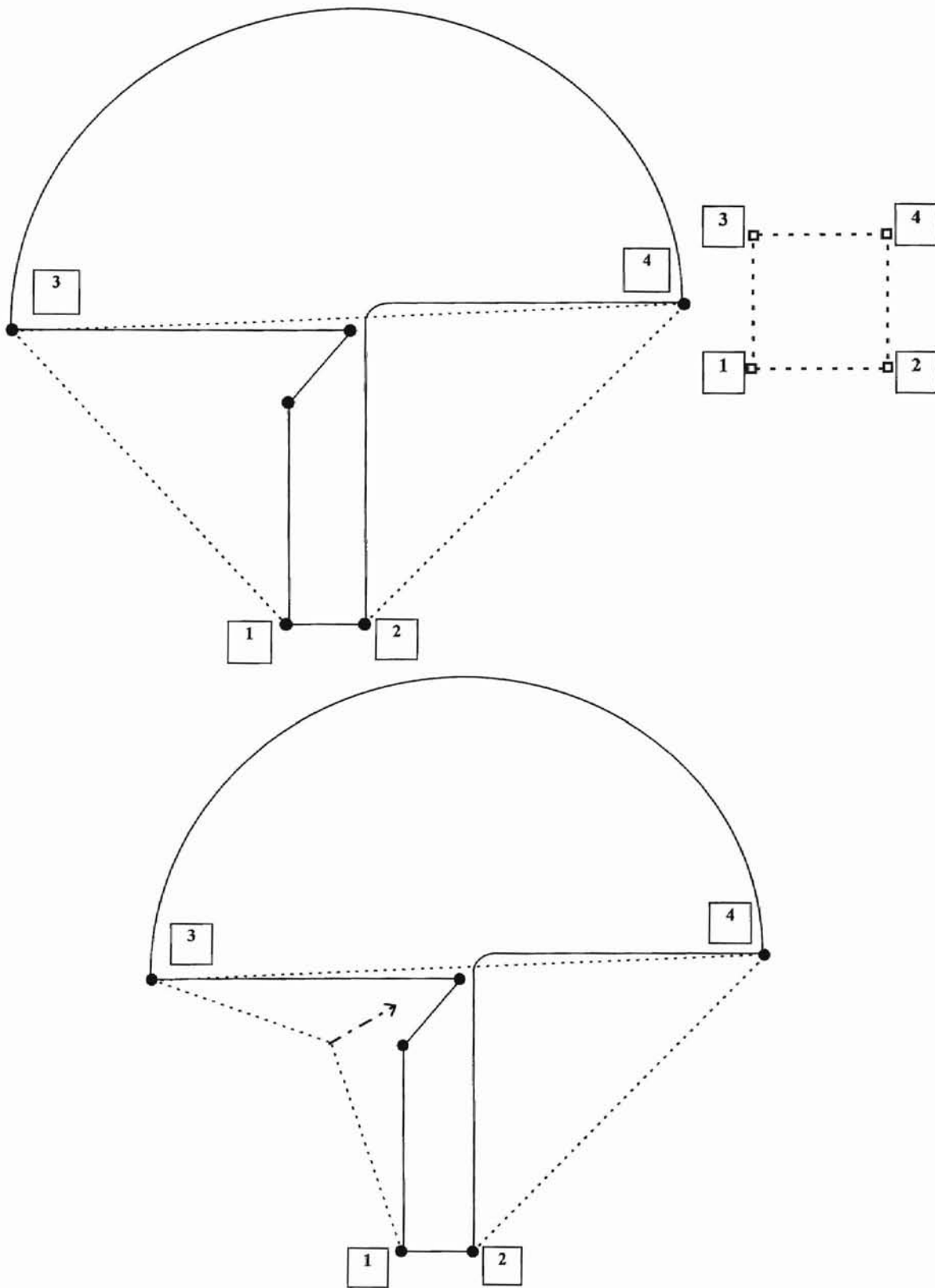
Figure A.4 Overlaying domain topology on the geometry using a face

Once the face is shaped to conform to the domain, the boundary conditions may be set at this point. (Note that these bcs may be changed later from within FLUENT/UNS). Select EDGES and then the B-COND : SET. We get a dialog window, which lists all the bcs available. Choose an edge, and it's boundary condition. It may be noted that all the edges are initially assigned as WALL.

The edge 1-2 is assigned to be PRESSURE-INLET, and the curved edge 3-4 is assigned PRESSURE-OUTLET. Exit out of the dialog by pressing CLOSE. The figure shows the final configuration.
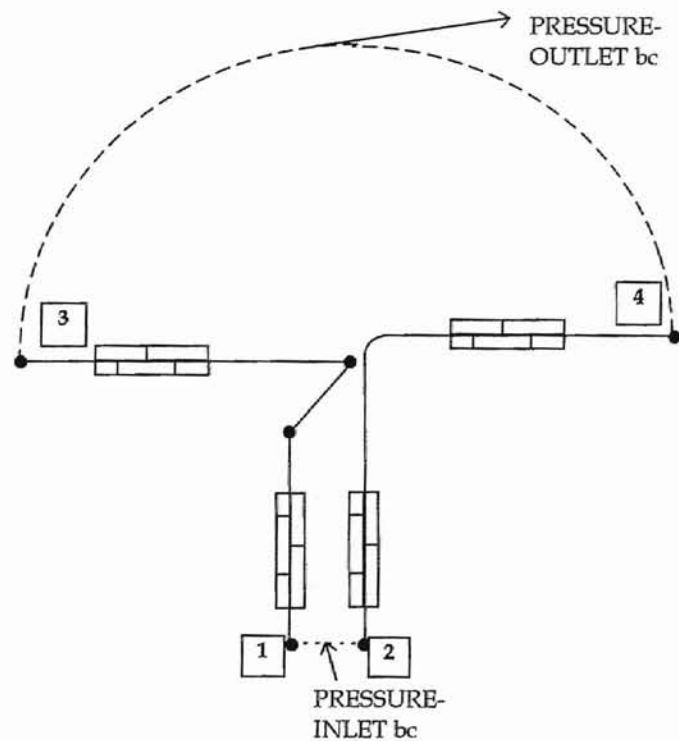
Figure A.5 Final configuration showing the boundary conditions

The next step is to create the overlying grid. It should be kept in mind that the solver actually "sees" only the grid and not the geometry during the solving process. Hence, the user should take care that the grid accurately models the geometry. This means that the grid should satisfy the following conditions :

1.   Grid should be dense in regions of anticipated high

            gradients, and quite coarse in other regions.

2.   Grid skewness should be kept lower than 0.70

3.   Gridlines must align with the flow direction

Choose BUNCH: SET TRI to set the number of nodes on each edge. The node distribution on the edge may be adjusted at this point. By default each edge gets at least 3 nodes. Choose an edge, and adjust the number of nodes and their distribution by dragging the control points in the curve diagram shown.

Figure A.6   BUNCH:SET-TRI option

In our model the nodes distribution is adjusted such that the mesh is

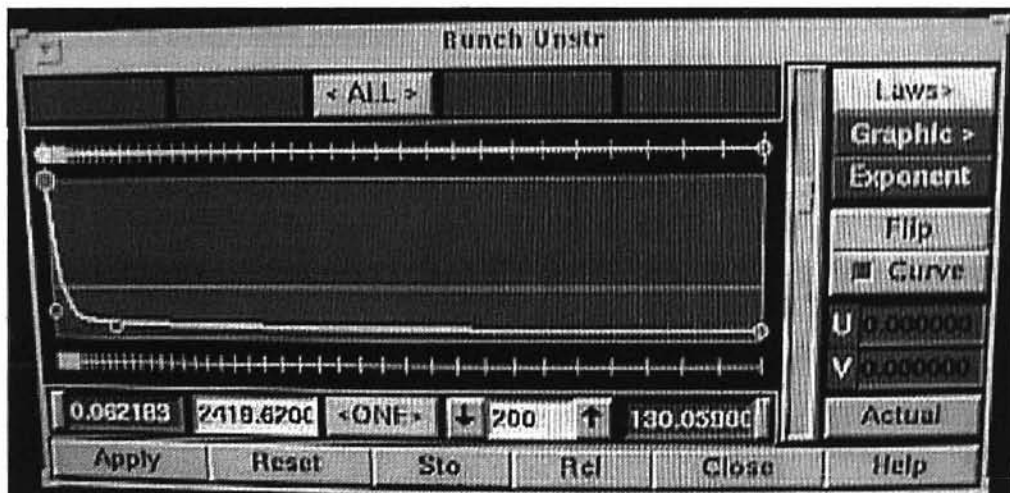highly dense near the nozzle, and gets coarser as we move away from it. After the distribution has been adjusted on all the edges, the grid may be generated by choosing MESH:CREATE. The grid generation proceeds with no user intervention. The generated mesh is shown in figure.

If the grid looks satisfactory, we may now use the option SAVE AND EXIT in the FILE menu to quit P-CUBE. Before proceeding to the next step, we need to translate the grid to suit FLUENT/UNS input format. We may do this by choosing the FLUENT/UNS INPUT option in the TRANSLATE menu in GeoMesh. Click on "Unstructured ", and click OK. You may want to change the name given to the mesh file at this point. In the next dialog, click on ALL to export all the grid domains to FLUENT/UNS format. Again click on OK to start the translation process.

Step 2 : Start the appropriate solver

In this step we will start the FLUENT/UNS solver to calculate the solution. We may do that either by choosing FLUENT/UNS from the APPLICATION menu, and then typing 2D in the following dialog box, or by typing

$ uns 2d <ENTER>

at the command prompt. Either way, UNS starts up, and is ready for calculation.

Step 3 : Import the grid

Before the grid can be read into the system, we need to read in the "scheme" file. This file has is a property database of a large variety of materials. This can be done by choosing FILE/READ/SCHEME. Choose the "propdb.scm" file and click on OK to read the file. Now, we are ready to read in the grid file.

Choose the READ/CASE FILE option from the FILE menu to read in the grid file. The solver verifies the mesh as it reads and displays some information about the mesh on the screen.

Step 4 : Check and scale the mesh, if necessary.

In our case, we find that the units we have used to create the mesh are in millimeters. At this point we might tell the solver about the units used to create the mesh. This may be done by choosing GRID/SCALE. Not that in the dialog box that comes up, the default unit is shown as meters. Change the "Mesh was created in :" to "mm". You may have to click on SCALE to scale the grid. The grid might be checked for any errors at this point by choosing GRID/CHECK. A typical output looks as follows.

Step 5 : Choose the models and equations to be solved

We start to define the solver parameters at this step. We start with choosing the appropriate models and equations to be solved. Choose DEFINE/MODELS to change the models to be used in the solving process. Under the VISCOUS OPTION, choose the RSM Turbulence Model and the non-uniform wall function. All other parameters may be left at their default values.

Since we expect to have higher than 0.3 times the Mach speed, we need to model a compressible flow. Hence turn on the "Heat transfer" option.

The equations to be solved (continuity, momentum, energy, etc,.) need not be changed in this case, because FLUENT/UNS dynamically changes the equations to solve, to properly reflect the models chosen.

Step 6 : Specify the material properties

The properties of the FLUID in the solution domain have to be set at this point by choosing DEFINE/MATERIALS. In the dialog box, click on PROPERTIES, and enable the "Compressible form of the ideal gas law". This will result in the density being calculated from the ideal-gas law. The operating pressure and temperature may be set at 14.123 psi and 296.3K respectively.

Step 7 : Specify the boundary conditions

We need to specify the boundary conditions by choosing DEFINE/BCS. The solver shows a dialog box with a list of available zones. Choose the following boundary conditions for the zones.

INLET-1

Choose the gauge pressure to the value required at the inlet (say, 0.1psi). This pressure is defined relative to the operating pressure. Set the x-direction vector to be 0 and the y-direction vector to be 1, because the direction of flow at the inlet is in the vertically upward direction. The temperature is set at 296.3K.

OUTLET-1

Choose the gauge pressure here to be equal to 0 psi (relative to the

operating pressure), referring to atmospheric conditions at the boundary. This simulates free space at the outlet. The temperature at the outlet is set at 296.3 K. This will result in isothermal conditions in the solution domain.

WALL-1

The temperature at the wall is set at 296.3K to maintain isothermal conditions. The material is set as Aluminium. The surface roughness is set to 1.1303e-03 mm. All other parameters may be left at their default values.

Step 8 : Adjust solution control parameters

The solution control parameters determine the way in which the solution is computed. They influence the solution accuracy and convergence. Since we are using an unstructured triangular mesh, we need to use second-order discretization to keep the numerical diffusion at a minimum. Hence choose SOLVE/CONTROLS/DISCRETIZATION, and choose SECOND-ORDER for all the solution parameters.

The next control parameter is the residual. The residual is the difference between the solution parameter, at consecutive steps. FLUENT/UNS uses the residual value to decide when to stop the calculations. Each solution parameter has a residual associated with it. By default it is 0.001. We need to change this value to improve the accuracy and to obtain a fully converged solution. Choose SOLVE/CONTROLS/RESIDUALS, and change the residual for k and ε to 5e-05.

This value has been found to yield converged solutions.

Another very important control parameter is the under-relaxation parameter. These parameters have a value between 0 and 1. They determine the rate at which the solution progresses. Keeping them high will result in a high rate of convergence, but may make the solution procedure unstable. Keeping them low, will reduce the unstability but will require more iterations. We have to strike a balance, to obtain stability and speed. In this case, the default under-relaxation parameters for the solution parameters have found to be optimum.

Step 9 : Initialize the flow field.

The flow field has to be initialized before starting calculations. This might be done by choosing SOLVE/INITIALIZE. Give the initial value for pressure field as 0.1 psi (same as the inlet pressure). The other parameters need not be changed. It might be noted that based on the value of the initial pressure field, the rate of convergence and the number of iterations required varies widely. For this model, it was found that the number of iterations with an initial pressure field of 0 psi, was about 5500 iterations, whereas that with a initial pressure of 0.1psi took only around 900-1000 iterations, resulting in a considerable resource savings.

Step 10 : Calculate the solution.

Now we are ready to start the iterations. Before doing that, we can switch the residual monitoring, to visually monitor the convergence process. This can

be done by choosing PLOT/RESIDUALS, and turning on the PLOT option in the dialog. The iterations might be started through SOLVE/ITERATE. The maximum number of iterations maybe set at 10000. Note that once the solution has converged FLUENT/UNS automatically stops the calculations. Once the calculations have started, a window opens up, which shows the residual behavior. If they show a downward trend, it means that we are having a converging (and favorable) condition. If the residuals show a continuing upward trend, we might have to lower the under-relaxation parameter of that solution parameter. The solving process can then be resumed from that point, without having to start from the beginning.

Step 11 : Post processing - Examine the solution

Once the calculations have stopped, we can examine the solution in a variety of ways. For instance, we may view the velocity vectors, contours of pressure distribution, etc. in the solution domain. We should also test the convergence by continuing the solution process, after reducing the under-relaxation parameters. If the solution is found to change, then it means that we do not have a fully-converged solution. In that case, we might have to continue the solution process.

Step 12 : If necessary, refine the grid and repeat the calculations

If the grid seems too coarse in regions where the parameters seem to have

a large gradient, we might have to refine the grid and repeat the calculations. FLUENT/UNS has a feature called grid-adaption, which helps in the process of refining the grid based on parameter gradient data available from the calculation results. We might choose that option under ADAPT/REFINE.

Though the procedure explained above is specific to the Coanda air jet model, the basic idea to create a model and solve it using Fluent should be the same. The user is advised to refer to the Fluent manuals for any future concerns, that might involve topics not discussed here.

VITA

Thirumal Sathia Prabhu

Candidate for the Degree of

Master of Science

Thesis: A COMPUTATIONAL STUDY OF THE COANDA EFFECT AND ITS IMPLEMENTATION IN WEB SUPPORT AND TRACTION.

Major Field: Mechanical Engineering.

Biographical:

Personal Data: Born in Thanjavur, India on the 15th of May, 1975 as the eldest son of Mr. T Sathiamoorthy and Mrs. S. Usharani.

Education: Received Bachelor of Engineering degree (Gold Medalist) in Mechanical Engineering from Bharathiar University, Coimbatore, India in May 1996.

Completed the requirements for Master of Science degree with a major in Mechanical Engineering at Oklahoma State University, Stillwater in May 1998.

Experience: Research Assistant in the Web Handling Research Center from August 1996 to May 1998.
Graduate Assistant in the Office of Business Research from January 1998 to May 1998.

Professional

Memberships: Phi Kappa Pi.
Tau Beta Pi, the national engineering honor society.
American Society of Mechanical Engineers.